

Chapter 2

LITERATURE SURVEY

2.1 Characteristics of jet

The turbulent flow is desired to increase the rate of transfer per unit area or to help dispersion of one fluid to another and to create more interfacial area, for most of mass transfer between gas and liquid. Dispersion of one fluid to another is a complex phenomenon and depends on many factors like velocity of jet, pressure difference, geometry of nozzle, temperature of both fluids, properties of fluid like their density, viscosity, surface tension, vapor pressure, etc.

The breakup of a liquid jet radiating into another fluid was been studied by many investigator since century. It has been stated by Plateau (1873) that jet breakup in segments having equal length of 2π times of the jet radius. Rayleigh (1879a) and (1879b) explained that hydrodynamic instability is responsible for the jet breakup. Weber (1931) studied the effects of the density of the ambient fluid and liquid viscosity. Further, Tomotika (1935) explain about an optimum ratio of viscosities of the jet to the ambient fluid at which jet attains the maximum growth rate. Chandrasekhar (1961) accounted the liquid viscosity as well as the liquid density, which was not considered by Rayleigh and mathematically proved that as the viscosity increases the breakup rate of jet reduces and drop size increases. They further conclude that breakup of viscous liquid jet is by capillary pinching mechanism under vacuum. (Lin and Reitz 1998)

2.1.1 Behavior of jet

Free jet

A free jet, after leaving the nozzle, will entrain the surrounding fluid, expand and decelerate. Approximately, total momentum which is conserved as jet momentum is transferred to the entrained fluid. In the literature it has also been defined that when the cross-sectional area of jet is less than $1/5$ then the cross section of surrounding region then jet is considered to be free jet in case of both fluid, surrounding fluid and jet fluid, are same. While the turbulent jet having Reynolds number greater than 2000 is considered to be a free jet. (Perry et al., 2007)

Jet length

The high velocity liquid jet coming out of nozzle situated at the top of ejector flowing through the stagnant fluid surrounding it maintains its identity for a substantial distance (Figure 2.1). It may is observed for the jet issuing from the nozzle having uniform and constant velocity that

- The velocity remain uniform and constant in the core
- the area of core decreases with distance from the nozzle,
- the core is bounded by an increasing turbulent jet, in which the radial velocity decreases with distance from the centerline of the jet,
- the core is shrinking and disappears at some distance from the nozzle,
- but the turbulent jet maintains its integrity further than the point at which the core disappeared however its velocity steadily decreases,
- the radial velocity in the jet decreases and a pressure increases in as per the Bernoulli principle

There is simultaneous surrounding fluid enters into the jet and is absorbed, accelerated and blended into the enlarged jet. This process is called entrainment.

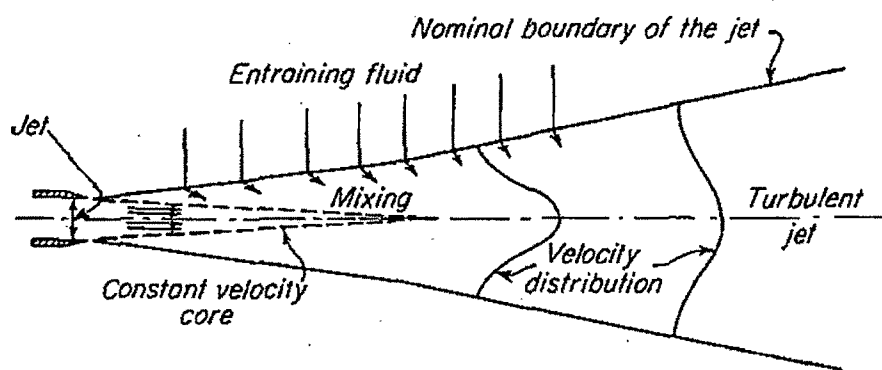


Figure 2.1 : Flow of a submerged circular jet (Rushton and Oldshue, 1953).

In this process there are also strong shear stresses at the boundary of the jet and the surrounding liquid. Due to these stresses strong eddies are generated at the boundary and create considerable turbulence, which causes the intimate mixing action. It is also established that liquid flow at high velocity and entrainment of large quantity alone do not sufficient for thorough mixing. Enough time and space is must for the streams to mix together satisfactorily by the mechanism of entrainment. (McCabe et al., 1993)

Liquid jet break-up length

Breakup length of round liquid jet was measured by Eroglu et al. (1991) in annular coaxial air streams. They further observed that the decreasing breakup length with increasing Weber

number and they also found that liquid jet length increases by increasing Reynolds number. They gave following expression:

$$\frac{L}{2a} = 0.5We_L^{-0.4}Re_g^{0.6} \quad (2.1)$$

Where a = central tube inner radius and L = liquid intact length. Here Weber (We) and Reynolds numbers (Re) are based on gas and liquid relative velocity.

In similar attempt numerical analysis of jet breakup is performed by Kazuya et al. (2004) using the Moving Particle Semi-implicit (MPS) method in x - y two dimensions. Effects of the Weber number and the Froude number on the jet breakup length agree well with experimental data. The breakup length with gravity is from 70 to 80% of the experimental data. They expressed L/D as the following expression:

$$\frac{L}{D} = 2.2We^{0.28}Fr^{0.78} \quad (2.2)$$

where L , D , We and Fr are jet breakup length, nozzle width, Weber number and Froude number, respectively. However, the coefficient 2.2 by the MPS method is a little smaller than experimentally obtained values 2.5 for alcohol and 3.0 for water.

Flow regions of free turbulent jet

Tuve (1953) and Davies (1972) have explained break up length differently. A turbulent free jet is normally considered to be consisting of four flow regions that are:

- Region of flow establishment is up to the 6.4 times nozzle diameter. In this region there is a core having conical shape and the velocity is same as at the discharge of the nozzle. As jet proceed away from the discharge of the nozzle, slowly boundary between jet and surrounding reduces to centerline. Here this region is considered to be terminated.
- Next transition region is up to the 8 times diameter of nozzle.
- Region of established flow is the foremost region of the jet. Here, the radial velocity profile is self-conserving with respect to centerline velocity.

- In terminal region centerline velocity reduces rapidly. For air jets, the residual velocity will reduce to less than 0.3 m/s which is considered to be still air.

Several researchers (Tie et al., 2011; Pfeifer et al., 2010; Leick, 2008; Yongyingsakthavorn et al., 2004; Smallwood and Gulder, 2000, Kufferath et al., 1999; Wolfe et al., 1964) have reported the jet behavior.

2.1.2 Types of primary atomization

The liquid jet behavior is a critical step in mass and heat transfer operations. There are mainly three categories of mechanisms (Meyers, 2006) of jet disintegration namely:

Mechanical primary atomization

Liquid jet is injected at high speed through a small hole in a gaseous medium at rest. This type of atomization is supposed to have very strong difference in pressure between the upstream and downstream of the orifice. This type of jet is also called free jet. This type of atomization of jet is used in jet ejectors.

Aerodynamic primary atomization

Liquid jet injected at low speed in the chamber surrounded by a gas jet injected at high speed. This type of coaxial jet is also called assisted jet. This type of atomization of jet is used in high energy venturi scrubber (HEVS).

Impact primary atomization

When atomization is performed by impact of two liquid jets or a liquid jet to a wall, it is called impact primary atomization.

The understanding of the phenomenon of primary atomization is still not clear due to the difficulty in observation of primary fracture of jet in the dense zone of the flow. Moreover there are strong changes in topology of interface and quick transfer between the phases in this zone very rapidly, alter the properties of the drops/bubbles before they reach experimentally observable conditions. However, recently due to the improvement of measurement techniques (holography technology and probes of optical fiber) understanding of the dense fog area has become possible.

The current study involves mechanical primary atomization by multi nozzle jet ejector. Review of literature published about mechanical primary atomization is given as under:

2.1.3 Mechanical primary atomization

Faeth (1999, 1990) and Reitz and Bracco (1986) have given exhaustive review of literature on mechanical atomization. Ohnesorge and Angew (1936) provided the first classification of different schemes based on the Reynolds and Ohnesorge numbers. Reitz (1978) clarified the uncertainty of classification proposed by Ohnesorge and Angew.

Lin and Reitz (1998) as well Atay (1986, 1987) discussed various regimes of breakup of liquid jets injected into both stagnant and co-flowing gases. Available criteria for the alteration from one regime to another have been reviewed by them. They proposed a convenient method of categorizing jet breakup regimes by considering the length of the coherent portion of the liquid jet or its unbroken length, L , as a function of the jet exit velocity, U , [Refer Figure 2.2(1) and Figure 2.2(2)].

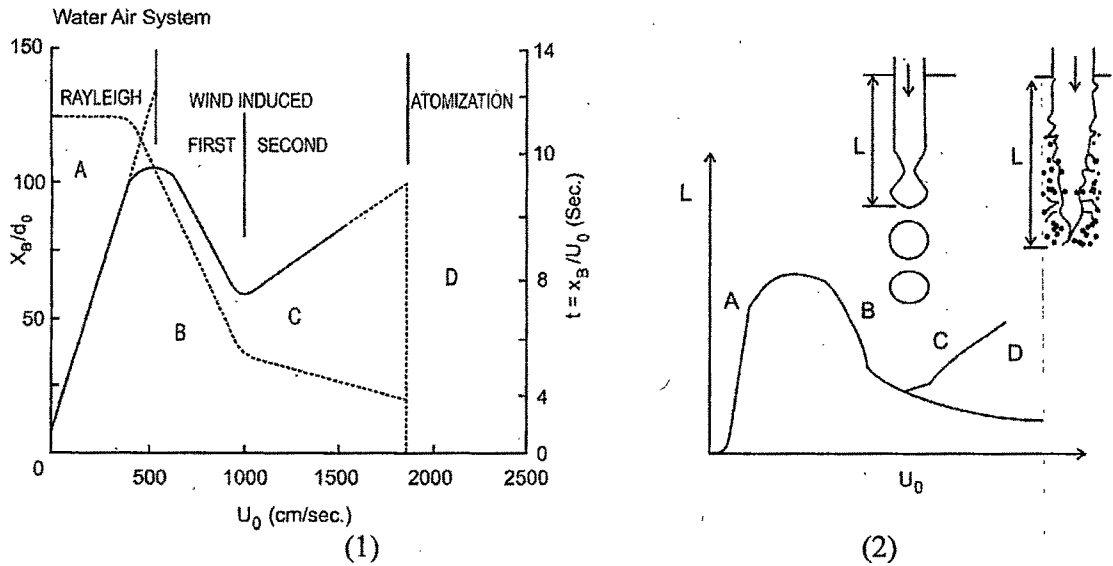


Figure 2.2 : Break up time and/or jet breakup length as a function of jet exit velocity

[Adopted from (1) Atay (1986), (2) Lin and Reitz (1998)]

They identified four main breakup regimes which were based on combinations of inertia of liquid, surface tension and forces of aerodynamic acting on the jet. The regimes are named as follows

- (1) The Rayleigh regime,
- (2) The first wind-induced regime,
- (3) The second wind-induced regime and
- (4) The atomization regime.

These regimes are summarized as in Table 2.1

Table 2.1 : Jet breakup regimes (Lin and Reitz, 1998 and Atay, 1986)

Type of Regime	Jet velocity U_0 , m/sec	Break up length X_B in terms of X_B/d_0	Diameter of drop, d	Webber no, $We_L = \frac{\rho_1 U^2 (2a)}{\sigma}$ $We_g = \frac{\rho_g U^2 (2a)}{\sigma}$
Rayleigh Jet Breakup Regime	0 – 5	10 – 110	$d > d_0$	$We_L > 8$ $We_g < 0.4$
First Wind Induced Breakup Regime	5 – 10	110 – 60	$d = d_0$	$0.4 < We_g < 13$
Second Wind Induced Breakup Regime	10 – 18	60 – 100	$d < d_0$	$13 < We_g < 40.3$
Atomization Regime	> 18	0	$d \ll d_0$	$40.3 < We_g$

* U is the relative velocity between jet and gas, d_0 = diameter of nozzle, $2a = d_0$

Region A and B of figure (2.2) shows that after the dripping flow regime ($We_L > 8$), the breakup length linearly increases in beginning as jet velocity increases till it reaches maximum and then start decreases. It is also clear that the drops are pinched of having comparable diameter to the jet. These two breakup regimes, which are understood properly, related to the Rayleigh and first wind-induced breakup regimes.

However, there is variation in observation about breakup-length trends beyond the first wind-induced breakup regime. Haenlein (1932) stated that the jet breakup length increases with increasing jet velocity again. [region C in Figure 2.2], and then suddenly reduces to zero [region D Figure 2.2] while McCarthy & Malloy (1974) reported that the breakup length discontinues shortening and elongation of the jet with changes in the jet velocity. Castleman (1931) observed that the breakup occurs at some jet diameters from the orifice, while DeJuhasz (1931) claims that disintegration begin within the nozzle itself.

Theories developed for jet breakup have been reported by various investigators as tabulated in Table 2.2.

Table 2.2 : References on jet breakup and primary atomization

References	Theory of jet breakup
Ranz (1956)	Breakup by balancing inertial forces with surface tension forces, neglecting viscous shear stress.
Fraser et al. (1962)	Hydraulic atomization of rapidly moving liquid sheet.
Reitz (1978,2004)	Atomization and other breakup regimes of a liquid jet
Ingebo (1991)	Liquid Jet breakup in sonic- velocity gas flow.
Frago and Chigier (1992)	Pulsating and super pulsating breakup process.
Chigier & Reitz. (1996)	Air- blast coaxial atomization.
Kankkunen et al. (1997)	Sheet breakup mechanism of black liquor.
Meier et al. (1997)	Breakup of very low velocity liquid jets.
Geschner et al. (2001, 2004)	Disintegration of sinusoidally forced liquid jet.
Herrero et al. (2007)	Air blast atomization of swirling viscous annular liquid sheet (alginate solution)

Tie Li et al. (2011), Tamaki et al. (2007, 2010) and Yongyingsakthavorn et al. (2004) have reported that there are still other parameters which effect the breakup of jet: physical properties of fluid, the nozzle geometry, the surrounding gas (stagnant or moving, atmospheric or pressurized).

2.1.4 Effect of various variables on liquid jet breakup

Effect of the environmental pressure

Reitz and Bracco (1986) noted that the atomization regime can be obtained for low-speed fluid when it is injected into a highly pressurized environment. The length of intact surface decreases with increasing environmental pressure to a certain value.

Faeth (1990, 1995), Tseng et al (1992a, b), and Ruff et al (1992) studied the structure of an atomized spray in a pressurized environment. Atomized spray in a pressurized environment shows a very dense area, called the liquid core, at the outlet of ejector. Chehroudi et al. (1985) found that the faster rate of mixing results in high pressures of the surrounding environment. However, these effects are relatively low. Faeth (1999) noted that

for $\rho_L / \rho_G < 500$ the aerodynamic forces influence the atomization. Similar study was also done recently by Kufferath et al. (1999).

Effect of turbulence

Properties of jet are highly dependent on the state of development of the turbulence at injector outlet. Faeth (1995) confirms this by varying the output conditions of the jet. It seems that mixing rates are increased greatly in the layer of liquid mixture with the degree of turbulence of the liquid jet. Wu et al. (1995) and Wu and Faeth (1995, 1993) proposed an analysis for fully turbulent jets developed at injector outlet, to estimate the average Sauter diameter (SMD) of drops produced early in the process of atomization and position of primary rupture. Wu et al. (1995) assume that the drops are formed when the kinetic energy of the smallest eddy is comparable to the energy of surface tension necessary to form a drop of similar size. This principle was already envisaged by Kolmogorov (1949). Similar effect of turbulence has also been studied by Kufferath et al (1999).

Effect of liquid viscosity

In general, increasing the viscosity of the fluid must tend to delay breakup of the liquid jet as it balances the forces of inertia. Indeed, this parameter is taken care in the calculation of the Reynolds number of the liquid. Reitz and Bracco (1982) studied the influence of the viscosity of liquid by varying the proportion of glycerol and water in the liquid phase. They showed that instabilities are strongly dampened when the viscosity increases resulting in the formation of a laminar liquid jet. The angle of the fog is not influenced by changes in viscosity. Finally, the position of the primary break shifts downstream. Lefebvre (1989) showed that the viscosity plays a role in the average diameter of drops formed. It was noted that the SMD increases with viscosity. Indeed when the viscosity increases, the internal turbulence of the fluid decreases and leads to an increase in wavelength of instabilities. This then results in a thickening (of liquid) produced disintegration as a result of the primary atomization. However, established atomization regime (high Reynolds number and Weber number), it appears that viscosity does not influence the primary atomization phenomenon but only influences the secondary breakage. Tamaki and Shimizu (2002) studied effect of kinematic viscosity (0.66×10^{-6} to 20×10^{-6} cSt). They studied the break up length and Sauter mean diameter (SMD) of highly viscous liquid sprayed at injection pressure up to 15 MPa. They concluded that the disintegration behavior of the spray and the spray characteristics are independent of kinematic viscosity. They have invented new atomization

enhancement nozzle (sharp edge with additional gap and bypass) which is able to atomize highly viscous liquid at low injection pressure. Similar conclusion was made by Krzeczowski (1980) in the study of measurement of liquid droplet disintegration mechanism. Contrary to this Herrero et al. (2007) concluded that when viscosity decreases there is shorter breakup length.

Effect of cavitation

The phenomena of cavitation can be expressed as the formation of vapor pockets (or bubbles) as a result of lowering pressure in a liquid jet. Cavitation is observed in nozzles of liquid atomizer. This question has been studied by many researchers. (Tamaki, 2009, Tamaki et al. 2001, 1998; Sou et al., 2009, 2007, 2006; Schmidt, 1997; Soteriou et al., 1995; Hiroyasu et al., 1991; Chaves et al., 1991; Bergwerk, 1959). As a result of many experiments conducted by many researchers, it has been determined that strong turbulence in the nozzle hole, induced by the cavitation phenomena, contribute enormously to the disintegration of the liquid jet. Sou et al. (2007) investigated the effect of cavitation on the flow in the nozzle and liquid jet atomization. They concluded the findings as (Refer Figure 2.3):

1. Cavitation in the nozzles and liquid jet can be classified into the four regimes
 - (i) No cavitation having wavy jet,
 - (ii) Developing cavitation having wavy jet,
 - (iii) Super cavitations having spray jet and
 - (iv) Hydraulic flip having flipping jet.

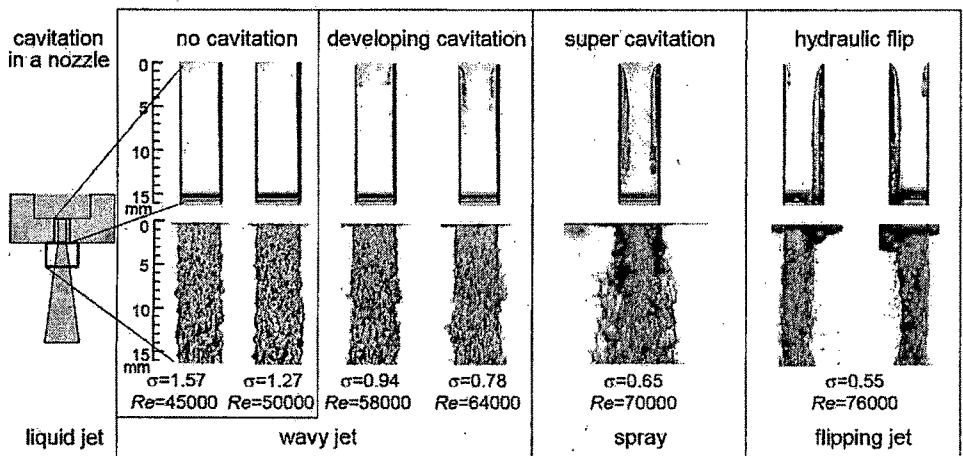


Figure 2.3 : Images of cavitation in a 2D nozzle and liquid jet (water) (Suo et al., 2006)

2. Liquid jet near the nozzle exit depends on cavitation regime
3. Cavitation and liquid jet are not strongly affected by Re
4. Surface tension (σ) and strong turbulence induced by the collapse of cavitation clouds near the exit play an important role in ligament formation.

In 2009, Sou et al. concluded after analyzing their results that cavitation length L_{cav}/L and jets are not strongly affected by Re but by σ .

Sou et al. (2008) after using the high-speed visualization concluded that since the pressure in the cavitating bubbles is much lower than ambient pressure, bubbles collapse either before reaching the surface of the liquid jet or immediately after reaching downstream of the nozzle. Park et al. (2008) noticed that super cavitation formation along the internal nozzle wall influences the external flow pattern and droplet formation.

Tamaki et al. (1998) observed that when cavitation takes place in a nozzle, it contributes greatly to the disintegration of the liquid jet. Leroux et al. (1996) studied the stability of Newtonian liquid jets and confirmed that the jet atomization is strongly influenced by the fastest growing wavelength in the radial direction

Effect of oscillating pressure field on liquid jet

McCormack et al. (1965) and Crane et al. (1964) studied the effect of mechanical vibration on the breakup of a liquid jet. They concluded that the application of mechanical vibration having the appropriate frequency range of small vibration, acceleration values can induce small pressure fluctuations and cause a capillary instability. Similarly with higher acceleration values there is substantial effect on radial velocity of liquid jet.

Barreras et al. (2002) studied the effect of ultrasonic vibrations on water atomization when excited with waves in the MHz range. They found that diameters of the resulting droplets are of the order of few microns. They used Malvern diffractometer to calculate droplet size distribution. There has been extensive study on the response of a bubble to a continuous oscillating pressure field. Neppiras (1980) explained that in the presence of oscillating pressure waves generated by an acoustic field, existing bubbles or cavities are subjected to both expansion and contraction.

Sindayihebura and Bolle (1998), Brennen (1995), Lin and Woods (1991), Knapp et al., (1970), McCormack et al., (1965) and Crane et al., (1964) have also studied the effect of vibration on the breakup of jet.

2.1.5 Secondary atomization

Physical process of disintegration of structures from the primary atomization to form multiple droplets is called secondary atomization. When a spherical liquid drop is subjected to a convective gas flow, it will initially become flattened due to pressure difference between the stagnation points at the front and rear of the drop and the lower pressure at the drop center. In addition to this distortion, the dynamic pressure exerted on the drop by gas flow also causes the drop to vibrate, and may cause it to breakup. The most important parameter for this phenomenon is the Weber number (We) calculated from the diameter of the large structures. Indeed, the main parameters that can affect the secondary atomization are acceleration of drop by external flow, shear due to the differential speed between liquid and gas and surface tension.

In fact, the secondary atomization controls the size of the drops in the spray. Two methods of disintegration processes are often treated separately, but, actually they are not clearly distinct from each other.

Faeth (1995) noted the existence of the two processes in the dense region close to the surface of the fast moving liquid jet and found a strong presence of small spherical drops confirming the rate of secondary atomization. The phenomenon of secondary atomization began as soon as the liquid structures (fragments, drops...) are grabbed up in liquid jet (results of the primary atomization) and become unstable. They are immediately subject to acceleration, due to momentum transfer with the gas.

Regimes of secondary atomization

Many experimental studies (Meyers, 2006; Gokalp et al., 2001, 2000; Gokalp and Chauveau, 2000; Zheng and Jasuja, 1994; Mansour and Chigier, 1994, 1993; Krzeczowski, 1980; Krauss, 1970; Ranger and Nicholls, 1969; Engel, 1958; Lane, 1951; Hinze, 1949) have identified different regimes of secondary atomization. The secondary atomization may be categorized better with the Weber number.

These modes of secondary atomization are generally distinguished as follow:

- **The deformation regime (case 1 of Figure 2.4)**

This type of atomization appears at lower Webber number. The deformation of the drop is a result of the imbalance between the dynamic pressure applied on the drop and the surface

tension force. While the speed of the flow surrounding drop increases the dynamic pressure applied on the drop also increases and that tends to distort it. The drop curvature increases in turn leading to the amplification of surface tension.

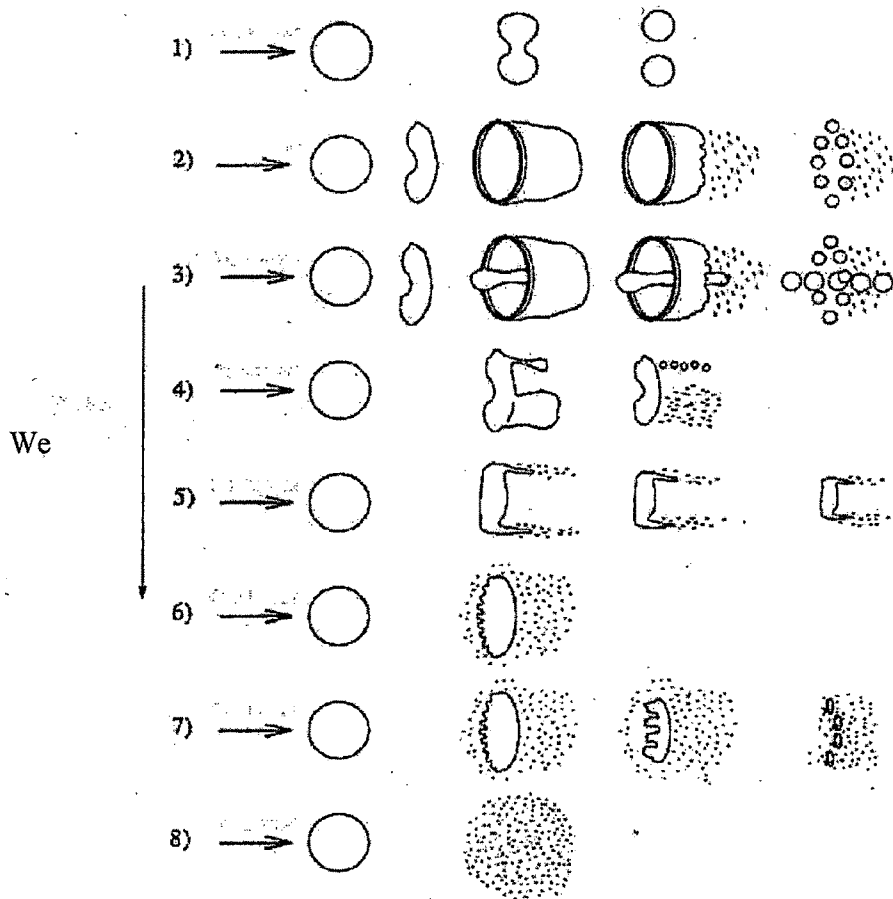


Figure 2.4 : Different schemes of secondary atomization (Meyers, 2006)

- **The "Bag break-up" regime (cases 2 and 3 of Figure 2.4)**

Bag break up occurs when the surface tension over compensates for the dynamic pressure applied on the surface of the drop. At breakpoint, flattened drop widens to form a sac which stretches in the direction of the flow. As a result of disruptions to the flow, the bag drills leading gradually to its disintegration into fine droplets.

- **The "Shear break-up" regime (cases 4 and 5 of Figure 2.4)**

There are two theories explaining this type of disintegration. The first (Hwang et al., 1996) assumes that the disintegration of the liquid fragment is due to the uprooting of the boundary layer that forms on the surface of the drop as a result of the shear with

the gas stream. The second theory (Hinze, 1955, 1959; Liu and Reitz, 1997) is based on the elongation of the ends of the drop in the direction of flow. Capillary waves are then formed on the surface of the drop which leads to the production of ligaments in the direction of the flow which will disintegrate drops.

- **The “Catastrophic break-up” regime (cases 6, 7 and 8 of Figure 2.4)**

This involves high speed. The process takes place in two stages. First low wavelength disturbances (type Rayleigh-Taylor instabilities) are formed on the upstream surface of drop because of its high acceleration. And then Kelvin - Helmholtz instabilities occur leading to the formation of several ligaments bursting into droplets.

There exist some other theories of secondary break up for different specific situations. Hopfinger (2001) considers only three scenarios of secondary breakage: breakage by shear, breakage by the turbulence of the gas and breakage by collision between the drops.

The criteria for transition between regimes

The transition between these different regimes is often defined through two dimensionless numbers. Many authors use Weber number and Reynolds number for distinguishing regimes.

Gelfand (1996) proposes the following criteria to test the regime:

- $0.2 \leq W_e/\sqrt{R_e} \leq 1$: deformation and rupture first type
- $1 \leq W_e/\sqrt{R_e} \leq 20$: failure by shear plan
- $W_e/\sqrt{R_e} \geq 20$: catastrophic failure

Gokalp et al. (2001) have also studied and presented the criteria of transition between regimes.

Time of breakup of drops to droplet

An important parameter characterizing the phenomenon of secondary atomization is the time of "breakup". This is the interval of time between the formation of drops and their disintegration to droplets. A first expression is given by Hinze (1955, 1959):

$$t_b = \frac{K_b d_i}{2\Delta U} \sqrt{\left(\frac{\rho_l}{\rho_g}\right)} \quad \text{where } 0.2 < K < 2 \quad (2.3)$$

O'Rourke and Amsden (1987) proposed a model (TAB: Taylor Analogy Breakup) based on the Taylor instabilities theory. The drop is regarded as a mass-spring system where the external force is the aerodynamic force of the gas, the call back spring force is the force of surface tension and the damping force of the system is fixed by the viscosity of the liquid. They get a similar equation as above where the value of constant K equal to $\sqrt{3}$. Similar study was done by other scientists also. Krzeczowski (1980) plotted time vs. We for methanol, water, ethanol, butanol, 50% aqueous solution of glycerin and glycerin and compared the results with other researchers (Littaye, 1943; Engel, 1958; Levich, 1962). The results are different from the earlier reported work. However Engel's formula fits somewhat to his results.

2.2 Bubble dynamics and interface phenomenon

This work is concerned mainly with the gas-liquid two-phase flow. Two-phase flow is defined as flow of a heterogeneous mixture of gas and liquid, where the fluid can be identified as macroscopic structure or in other words the fluids in a two-phase flow are not homogeneously mixed at a molecular level, but macroscopic regions of the fluid like droplets, bubbles, slugs, liquid films, ligaments, etc. can be observed. Typical examples of gas-liquid multiphase flow are bubbly, spray, and stratified flow where fluids are separated by a free surface like in annular and slug flow regime of gas-liquid two-phase flow in pipes and channels. Two-phase flow plays an important role in mass and heat transfer. Particularly for mass transfer operation high interfacial area is of most concern. To create high interfacial area the dispersion of one fluid into another is required. To study the dispersion of gas in liquid the knowledge of bubble size and bubble size distribution, bubble breakup and coalescence processes is necessary. Dispersion of one fluid into another is a complex phenomenon and is dependent on many factors like velocity of jet, pressure difference, geometry of nozzle, temperature of both fluids, properties of fluid like their density, viscosity, surface tension, vapor pressure, etc.

2.2.1 Flow pattern

Gas-liquid two-phase flow can be classified in four types: (a) Homogeneous bubbly flow (b) Heterogeneous churn flow (c) Slug flow and (d) Annular flow. Shown in Figure (2.5), and further summarized in Table (2.3).

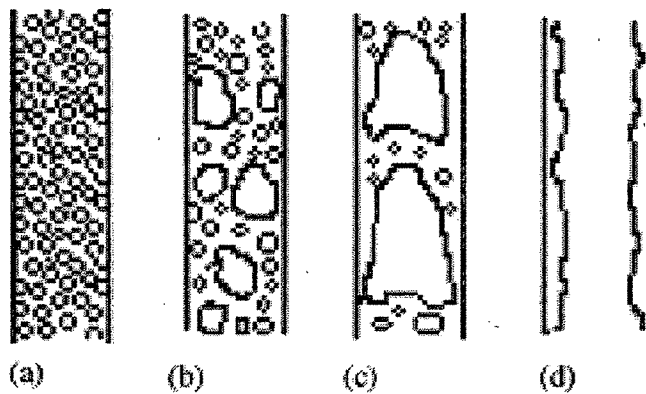


Figure 2.5 : Flow pattern in vertical column [(a) homogeneous bubbly flow (b) heterogeneous churn flow, (c) slug flow and (d) annular flow] (Mandal et al., 2004)

Table 2.3 : Flow patterns for gas-liquid two-phase flow in horizontal and vertical pipes : dependence on the gas volume fraction (Frank, 2005)

Gas volume fraction, (ϵ_G)	Horizontal pipe flow	Vertical pipe flow
<div style="display: flex; align-items: center;"> <div style="flex: 1; text-align: center;"> <div style="width: 100%; height: 100%; border-left: 1px solid black; position: relative;"> <div style="position: absolute; top: 0; bottom: 0; left: 0; right: 0; background: linear-gradient(to bottom, transparent 49%, black 49% 51%, transparent 51%);"></div> </div> </div> <div style="flex: 1; text-align: center;"> <div style="width: 100%; height: 100%; border-left: 1px solid black; position: relative;"> <div style="position: absolute; top: 0; bottom: 0; left: 0; right: 0; background: linear-gradient(to bottom, transparent 49%, black 49% 51%, transparent 51%);"></div> </div> </div> </div>	Finely dispersed bubbly flow	Finely dispersed bubbly flow
	Slug flow / plug flow	Disperse bubbly flow with near wall void fraction maximum
		Disperse bubbly flow with breakup & coalescence; gas volume fraction core peak
	Stratified flow with free surface (smooth, wavy, etc.)	Taylor bubble or slug flow
		Churn turbulent flow
High gas volume fraction	Annular / wall film flow	Annular / wall film flow
	Droplet flow	Droplet flow

Some researchers have further extended the classification to include froth, mist flow, etc. Frank (2005) explained that disperse bubbly flow is characterized by a characteristic bubble diameter (mono dispersed bubbly flow). Disperse bubbly flows have small to moderate gas

volume fraction; bubbles have varied shape (spherical, ellipsoidal, spherical cap bubbles). Hence the development of mathematical model must consider the flow morphology of disperse bubbly flow.

Although, flow regime primarily depends upon the gas superficial velocity and column diameter, liquid viscosity sometimes plays the prime role. In bubbly flow, the bubbles are quite uniform in size and they move in an orderly fashion with little collision among bubbles and the liquid is mildly stirred by the bubbles. Yamagiwa et al. (1990) observed that in case of co-current down flow, flow behavior changed from non-uniform bubbling flow to uniform bubbling flow when superficial liquid velocity increases and then to churn turbulent flow. This uniform bubbling flow was again obtained with further increase of liquid velocity.

Kedoush and Al-Khatib (1989) studied flow patterns with air-water flow in 3.8 cm I.D. pipe. They reported that transition from bubbly to slug flow occurs when $\varepsilon_G = 0.3$ (ε_G is gas hold up) and slug flow appears in the range $0.3 \leq \varepsilon_G \leq 0.7$. Mandal et al. (2004) studied ejector-induced co-current down flow system where gas flow rate is primarily controlled by liquid flow rate for a particular gas-liquid mixing height. They found that if liquid velocity increases significantly gas bubbles coalesce which leads to increase in buoyant force and hence they move upward rapidly and change to churn flow, slug flow, etc. However, for co-current down-flow system homogeneous bubbly flow regime is the better selection, otherwise it is quite difficult to move the bubbles in the downward direction. The operating range of the liquid flow rate for bubbly flow was 2.0×10^{-4} – $3.53 \times 10^{-4} m^3/s$ and the corresponding air entrainment rate varied from 0.40×10^{-5} to $9.0 \times 10^{-5} m^3/s$.

Zahradnik and Fialova (1996) observed a remarkable change when the superficial gas velocity is increased from $0.04 m s^{-1}$ (Refer Figure 2.6). The homogeneous bubble regime is changed and transition bubbling regime starts. In a similar study Rice and Littlefield (1987) also observed that the homogeneous bubbling regime ("ideal bubbly flow") was maintained up to gas superficial velocity equals $0.04 m s^{-1}$. Bakshi et al. (1995) identified that the transition from the homogeneous to the heterogeneous bubbling regime at gas superficial velocity $> 0.04 m s^{-1}$.

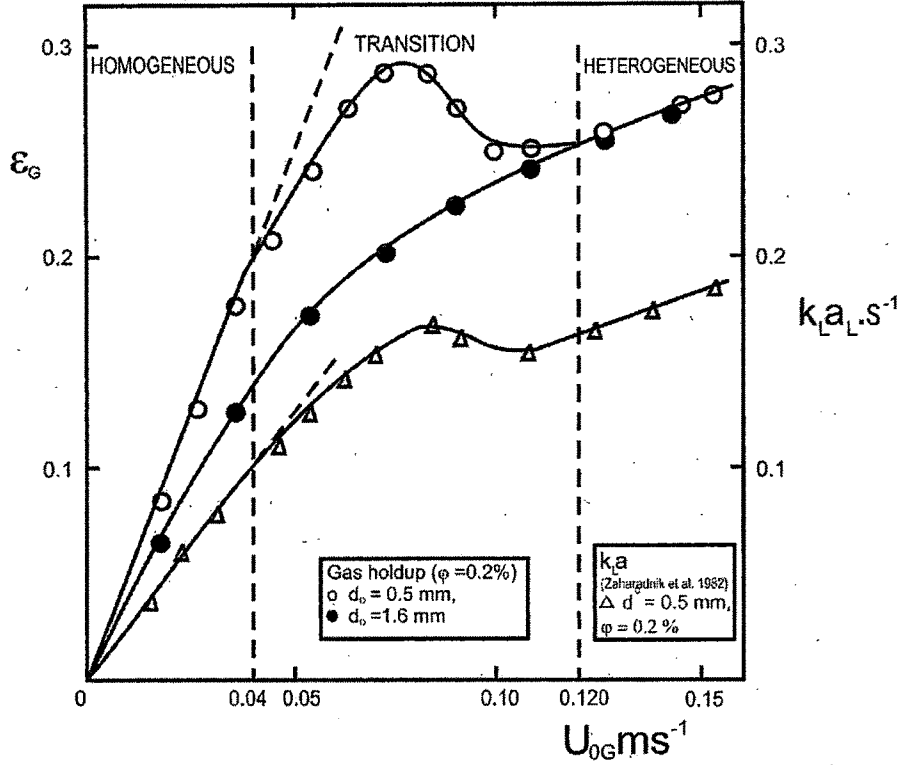


Figure 2.6 : Gas holdup and $k_L a$ as function of the superficial gas velocity; (Zahradnik and Fialova, 1996)

2.2.2 Bubble size

Under no circumstance fluid jet produce the liquid droplet/bubble of uniform diameter. In the study of jet ejector as gas-liquid contactor, the bubble size is a factor of utmost concern. Bubbles of uniform size are difficult to generate hence “mean bubble size” can be taken as a measure of the quality of the disintegration process. It is also convenient to use mean bubble size in calculations such as multiphase flow and mass transfer processes (Lefebvre, 1989).

In the literature (Lefebvre, 1989) average or mean bubble/particle/droplet diameter, $d_{i,j}$, is defined as

$$d_{i,j} = \frac{\int_0^\infty d^i f(d) dD}{\int_0^\infty d^j f(d) dD} \quad (2.4)$$

where d is the diameter and i and j take any value according to the effects considered (e.g. 3 and 2 for SMD, 1 and 0 for arithmetic mean diameter, 2 and 0 for surface mean diameter, 3 and 0 for volume mean diameter). There are many definitions of bubble size which cause confusion. However standard texts (Liu, 2000; Lefebvre, 1989) have summarized different

definitions, given by different researchers from time to time in their work. Out of them the most commonly used definition for “jet ejector” is d_{32} . It is defined as the diameter of a sphere that has the same volume/surface area ratio as a bubble of interest. Several methods have been devised to obtain a good estimate of the d_{32} . In the case of jet ejector studies, d_{32} is found most suitable mean diameter which is also known as Sauter mean diameter (SMD). This diameter has been established most appropriate because it gives the mean value in terms of volume / surface ratio. This relationship is the most suitable because the mass transfer takes place on the surface of droplets/bubbles and the acceleration caused by the drag forces. The drag force is proportional to the projected area of the bubble. Due to this, most of the cases bubble sizes and correlations for jet ejectors are presented in terms of d_{32} . Sauter mean diameter, d_{32} , can be computed using the following equations:

$$d_{32} = \frac{\sum N_i d_i^3}{\sum N_i d_i^2} \quad (2.5)$$

$$d_{32} = \frac{\int_0^\infty d^3 f(d) dD}{\int_0^\infty d^2 f(d) dD} \quad (2.6)$$

$$d_{32} = \frac{\int_0^\infty \left[d^3 \frac{dN}{dD} \right] dD}{\int_0^\infty \left[d^2 \frac{dN}{dD} \right] dD} \quad (2.7)$$

d_i is the diameter of a single bubble and N_i is the number of bubbles of diameter d_i .

2.2.3 Bubble size distribution

Practically in any gas-liquid two-phase system, gas is either entrained by plunging liquid jets or some time enforced to enter liquid media, do not generally produce dispersion of uniform bubble size at any given operating condition. On the contrary the plume of bubble can be regarded as a spectrum of bubble sizes distributed about some arbitrary defined mean value. In the two-phase gas-liquid system, there is simultaneous coalescence and breakup of bubble which are considered to be responsible for the variation in bubble sizes throughout the system.

Arranging the drop size data into a mathematical representation is referred to as drop size distribution. The mathematical representation is most often dependent on the analyzer used. Recently, however, some analyzer manufacturers have allowed the user to select

from a list of distribution functions rather than a default drop size distribution function (Schick, 2006).

Accurate knowledge of bubble size distribution as a function of operating conditions of the system is a prerequisite for the fundamental analysis of mass transfer.

There are various distribution functions applied by different investigators. But no single distribution function can correlate all experimental measurement data of bubble sizes. It is also known that none of known distribution functions is universally superior over any other for representing bubble size distribution.

Various distribution functions have been used to fit the existing experimental data. The most commonly used functions are; Rosin-Rammler, Nukiyama-Tanasawa and modified functions such as: upper-limit, logarithmic-normal, and chi-square (Li and Tanki, 1988, 1987). There are also some other distribution functions which were utilized by different researchers like- normal, root normal, gamma distribution, etc.

Because of the natural "cocked hat" shape of typical distribution data, the most logical curves used for representing the data have variations of negative exponentials. That gives an appropriately shaped "tail" in the large diameter end of the curve. However, pure negative exponentials also have an unrealistic finite count at zero diameters, so it must be corrected to give a second tail at the smaller diameter end. This second tail must end with a zero value at zero diameter. Different researchers have modified these correlations using different constants. (Dennis, 1966)

The bubble size distributions were measured at different axial positions of the column under steady state of a homogeneous bubbly flow. Various analytical distribution functions were tested by statistical software (SAS) for their adequacy in representing the observed bubble size distributions. It was found that the logarithmic normal distribution provided the most reasonable fittings for all the positions.

The probability function for logarithmic normal distribution $f(D)$ is given by the expression

$$f(D) = \frac{dN}{dD} = \frac{1}{\sqrt{2\pi}DS_g} \exp \left[-\frac{1}{2S_g^2} (\ln D - \ln \bar{D}_{ng})^2 \right] \quad (2.8)$$

where \bar{D}_{ng} is the number geometric mean droplet diameter and S_g is the geometric standard deviation

Azad and Sultan (2006) developed a numerical model for bubble size distribution for both breakage and coalescence in turbulent gas liquid dispersion. Two-step mechanisms are considered for both breakage and coalescence of bubbles. They structured the bubble breakage as the product of the bubble-eddy collision frequency and breakage efficiency in gas-liquid dispersions. Similarly the coalescence function was considered as the product of bubble-bubble collision frequency and coalescence efficiency. They claim that their model is better than previous efforts as their model overcomes several limitations observed such as empirical parameters, narrow range of operating conditions and narrow range of geometries. The predicted bubble size distribution by their model and the experimental data reported in the literature are in good agreement. The percentage of error obtained for the average bubble size was found within $\pm 17\%$. Frank (2005) and Silva et al. (2011) have also done similar work.

Cao and Christensen (2000) studied bubble collapse in a binary solution with simultaneous heat and mass transfer having non-spherically symmetrical condition. They applied a numerical technique to solve the axisymmetric moving boundary problem.

2.2.4 Measurement techniques of bubble size

Various measurement techniques have been developed and applied with different degrees of success. It is desired that the measurement techniques of bubble properties should be non-interfering and should not create disruption to the flow pattern. An ideal measurement technique should have large range of capability to measure both the spatial and sequential distribution. The measurement technique should be capable to tolerate wide variations in bubble properties at some extreme conditions present in flow in different engineering applications. It should also be able to acquire adequate representative samples so that reasonable measurement accuracy is ensured. (Akafuah, 2009)

For the analysis of the measurement of results of rapid sampling and data processing means are needed. As there is fast breakup and collisions of bubbles taking place, the sampling, data acquisition and processing system must also be fast enough.

The measurement techniques for droplet/bubble sizing may be grouped conveniently into four primary categories:

- Mechanical methods
- Electrical methods

- Optical methods
- Acoustical methods

Though mechanical and electrical methods are relatively simple and low cost, optical methods are being developed and are finding wide range of applications in two-phase flow characterization (Vamos, 2010; Kashdan et al., 2007, 2000; Black et al., 1996). An acoustical method has been evaluated for the measurements of fine bubbles. Table 2.4 summarizes the optical methods of measurement techniques.

Table 2.4 : Optical methods of characterization of two-phase flow

Categories	Methods	Size range (μm)
Imaging	Photography	$\geq \sim 5$
	Videography	-
	Holography	5 – 1000
Non Imaging	Light-scattering Interferometry	5 – 3000
	Phase-Doppler Anemometry	0.5 – 3000
	Light intensity deconvolution technique	0.2 – 200
	Light scattering technique	10 – 250
	Malvern particle analyzer	1 – 900
	Polarization ratio particle sizer	-
	Intensity ratio method	-
	Phase optical-microwave method	-
	Dual-cylindrical wave laser technique	-

2.2.5 Correlations for entrainment, bubble diameter, drag force and gas hold-up

The mean bubble size d_{32} is related to the pressure drop, gas ratio and liquid flow. The interfacial area and d_{32} both mainly depend on the local gas hold ups. The gas hold up is influenced by presence or absence of swirl body. Simonin (1959) proposed a quasi-theoretical relationship between the bubble diameter and the entrainment ratio for the air-water system:

$$d_v = 4.3 \times 10^{-3} \left[\frac{Q_A}{Q_w} \right]^{1/3} \quad (2.9)$$

The bubble volume-equivalent diameter, d_v , is expressed in meter. Equation (2.9) shows a moderate effect of entrainment ratio and was tested with experimental data by Ciborowski and Bin (1972), giving reasonable agreement.

Ohkawa et al. (1986) studied the flow characteristics and performance of a vertical liquid jet with down comers in an air-water system. Sheng and Irons (1995) made an attempt to model the bubble-breakup phenomenon in which the bubbles greater than critical size was allowed to subdivide into smaller (daughter) bubbles. The critical size was determined from the combined Kelvin-Helmholtz and Rayleigh-Taylor instability theory (Kitscha and Ocamustafaogullari, 1989) as

$$d_{vb} = 6.45 u_g \left[\frac{\sigma}{\rho_l g^3} \right]^{0.25} \quad (2.10)$$

where d_{vb} is the critical (volume-equivalent) diameter of the bubble, σ is the surface tension, g is the gravitational force and u_g is the rise-velocity of the bubble. The local breakup probability was assumed to have a Gaussian distribution. A random number generator is used to determine whether a particular bubble broke up or not. If this was the case, the number and size of the daughter bubbles were also calculated with a random number generator according to a predefined distribution. Further breakup of daughter bubbles was also permitted.

Similarly Baier (2001) developed following equation for calculating bubble diameter produced by jet ejector used in loop reactor.

$$d_{32} = 50.5 \cdot \left[\frac{\rho_G}{\rho_L} \right]^{-0.1} \cdot \left[\frac{g}{V_L^2} \right]^{-1/3} \quad (2.11)$$

where V_L is liquid batch volume.

Evans et al. (1992) discussed the applicability of the familiar model based on a critical Weber number, We , defined by the energy dissipation rate per unit volume of the mixing zone, which enables prediction of the maximum bubble size generated within the mixing zone at the top of a plunging liquid jet bubble column. A final expression for the maximum stable bubble diameter is given by

$$d_{b,max} = \rho_L^{-1/5} E^{-2/5} \left[\frac{We_c \sigma}{2} \right]^{3/5} \quad (2.12)$$

where E is the specific energy dissipation rate (per unit volume).

Ceylan et al. (2001) proposed the relationships to predict drag coefficient which is applicable for the solid spherical or cylindrical particles (in the range of $0.1 \leq Re \leq 10^6$) and for the deformable particles (drops and bubbles in the range of $0.1 \leq Re \leq 10^4$.) They presented their data with respect to Reynolds number and Bond number. Bond number is defined as

$$B_0 = \frac{(\rho_L - \rho_G)L^2g}{\sigma} = \frac{\text{gravitational force}}{\text{surface tension force}} \quad (2.13)$$

The predicted coefficients were in good agreement with the experimental data given in the literature. (Figure 2.7)

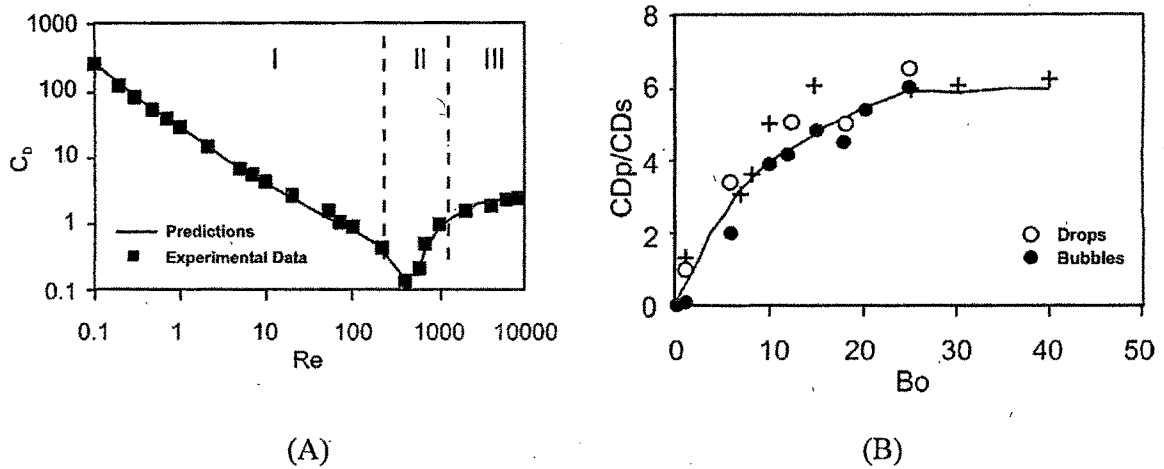


Figure 2.7 : (A) The dependence of drag coefficient on Reynolds number for the deformable particles. (B) Dependence of the drag coefficient on Bond numbers (Bo) for the deformable particle (Ceylan et al., 2001)

Havelka et al. (1997) studied the effect of swirl, number of nozzles and aspect ratio on gas suction rate and gas hold up in the ejector. They observed that multi nozzle having 4 nozzles, pitch 9.2 mm (ratio of pitch to nozzle diameter = 1.84) and aspect ratio 5, yielded higher value of gas suction rate than single orifice nozzle. Their results are in good agreement with findings of Panchal et al. (1991) who observed that in absence of swirl, multi nozzles yield higher suction rate at optimum pitch $l_d = 2D_N$.

Mandal et al. (2005a,b) have also investigated gas holdup, bubble size distribution and interfacial area. They found that bubble sizes have a logarithmic-normal probability distribution for any axial positions of the column. They compared geometric interfacial area obtained from Sauter mean bubble diameters and overall gas holdup with the interfacial area obtained by chemical method. Mandal et al. (2004) have also done similar study for non-Newtonian liquid.

Zahradnik and Fialova (1996) compared mixing data obtained by them with corresponding dependences of gas holdup and k_La on the superficial gas velocity.

2.2.6 Factors affecting the bubble size

Baier (2001) observed no significant differences of the mean bubble size (d_{32}) by changing ejector configuration and power input within the operating conditions used in the experiment (Figure 2.8).

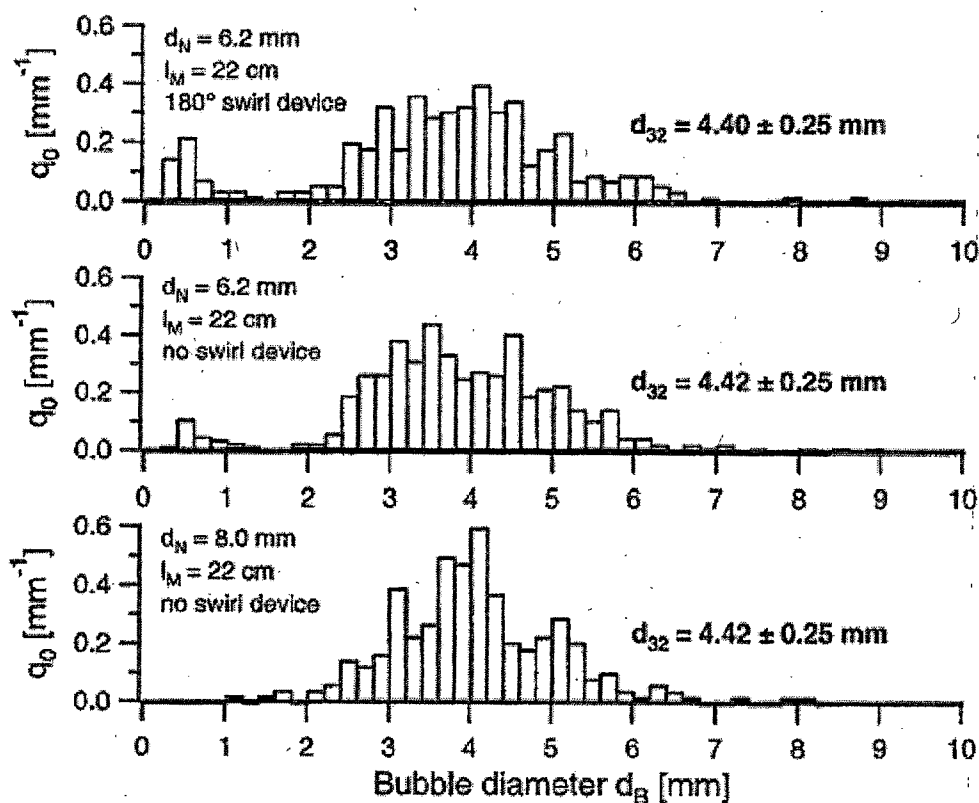


Figure 2.8 : Bubble size distributions at different reaction mixer configurations
(Baier, 2001)

Their findings are in good agreement with other published data. (Pawelczyk and Pindur, 1999; Dutta and Raghavan, 1987). Havelka et al. (1997) studied up-flow ejector loop reactor and observed axially and radially uniform bubble size distributions. Bin (1993) has extensively reviewed a large number of studies carried out on plunging liquid jet systems. For the air/water system and found that the secondary bubbles were formed very quickly and had diameters of about 4 mm, practically independent of the jet velocity and the nozzle diameter.

Baier (2001) studied the effect of electrolyte solutions on the average bubble size and observed that electrolyte solution have 10 time smaller bubbles than pure water. (Figure 2.9). This led to a strong increase of both $k_L a$ and the gas holdup. The estimated specific surface area considering mean bubble diameter (d_{32}) $\sim 700 \mu\text{m}$ is about 1500 and 6000 m^{-1} .

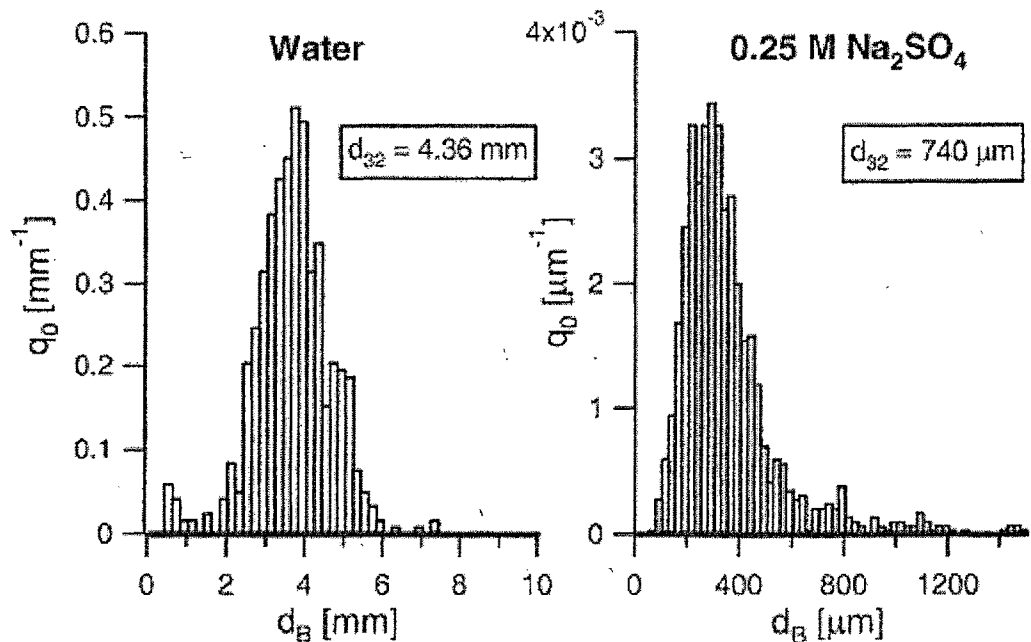


Figure 2.9: Characteristic bubble size distributions in water and in the 0.25 M Na_2SO_4 solution (Baier, 2001)

There are studies on the effect of gas density and operating pressure on average diameter. Baier (2001) found that system pressure and molecular weight of carrier gas have a significant influence on the bubble size. With increasing pressure and molecular weight of the gas component the Sauter bubble diameter decreases and the bubble size distribution becomes more narrow (see Figure 2.10 and 2.11). A strong correlation between the gas density and the Sauter bubble diameter can be identified.

The Sauter bubble diameter decreases with increasing gas density, i.e. the influence of the system pressure and the gas type can be fully attributed to changes of the gas density. In other words: If different gases of the same density are used, comparable bubble size distributions and Sauter diameters are obtained.

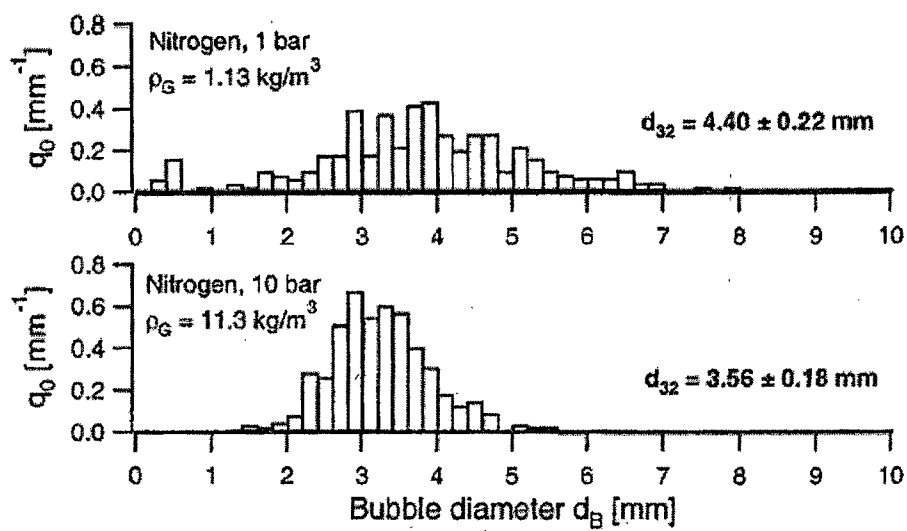


Figure 2.10: Bubble size distributions with nitrogen at different pressures (Baier, 2001)

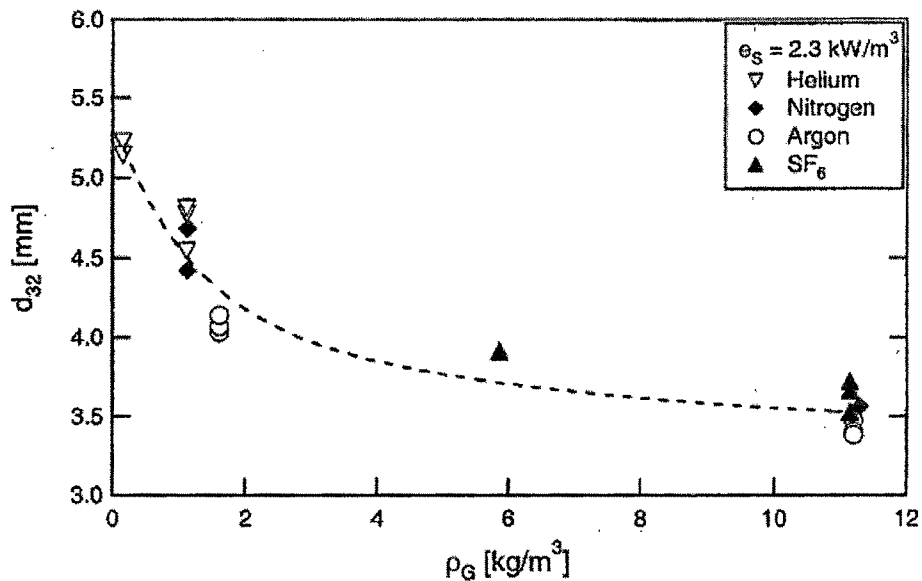


Figure 2.11: d_{32} versus the gas density (Baier, 2001)

Zheng et al. (2010) used PIV to measure local bubble size distribution, gas–liquid interfacial area and gas holdup in an up-flow ejector, based on the water-air system with different liquid

and gas flow rates under the presence/absence of the swirl body. They observed there is the formation of “bubble chain” in the ejector with swirl. The mean bubble sizes in the absence of swirl body are smaller than that in the presence of swirl under different operating conditions. The gas holdups and interfacial area are larger without swirl than those with swirl. Similar conclusions are also presented by Baier (2001).

2.3 Performance of venturi scrubber

Jet ejectors have been successfully used for polluted gas cleaning application over last many decades due to their capability of handling gas containing pollutants such as vapor, gaseous, and solid/liquid aerosols up to $0.1\ \mu\text{m}$ size. However they have inherent disadvantage of high pressure drop across the system which results in high fan/pump operating cost. But this disadvantage is compensated by their significantly less capital and maintenance costs compared to other wet scrubbers with comparable collection efficiencies. Since last six decades investigators have focused their attention to optimize the performance of venturi scrubbers.

Economopoulou and Harrison (2007), Viswanathan et al. (2005), Ravi et al. (2003), Gamisans et al. (2002), Ananthanarayanan and Viswanathan (1998), Singh et al. (1974) and Bhat (1972) have investigated the performance of jet ejectors. A jet ejector when used as a scrubber is considered to have given optimum performance when its desired scrubbing efficiency is achieved at minimum pressure drop. Models to predict pressure drop and scrubbing efficiency are required for optimization of performance of jet ejector. Pressure drop and scrubbing efficiency are complex functions of gas velocity, liquid-to-gas ratio, ejector geometry (shape and number of nozzles, area ratio, throat diameter, throat length, projection ratio, angle of divergence and convergence), operating and suction pressure, properties of gas and liquid (temperature, concentration, diffusivity, viscosity, surface tension, etc.), reactivity of fluids, variation in composition of fluids, etc. Most of researchers have presented their data graphically in dimensionless form. The equations governing scrubbing efficiency are either empirical or based on dimensional analysis. Recently some investigators (Taheri and Mohebbi, 2008) tried to utilize modern technique like artificial neural networks using a genetic algorithm for predicting collection efficiency in venturi scrubbers. Many researchers applied CFD method to understand the hydrodynamics. It is

common conclusion that CFD is an efficient tool for predicting the hydrodynamics and mass transfer characteristics of an ejector as it gives comparable result with experiments.

Venturi scrubbers are broadly classified into two groups viz. High Energy Venturi Scrubber (HEVS) and Ejector Venturi scrubber (EVS). As far as their performance is concerned HEVS may be differentiated from EVS as given in Table 2.5.

Table 2.5 : Performance of HEVS versus EVS

High Energy Venturi Scrubber (HEVS)	Ejector Venturi Scrubber(EVS)
Gas and liquid both are introduced in scrubber by external mechanical device.	Primary (Motive) fluid is ejected in venturi scrubber at high velocity by external mechanical device; another fluid is drawn in by kinetic energy of primary fluid.
L/G ratio is very low	L/G ratio is always high
Gas velocity in throat is dominant to break up liquid into droplets	Velocity of primary fluid at the discharge of nozzle/nozzles atomizes secondary fluid
Pressure drop and collection efficiency are studied as functions of operating conditions like L/G ratio, gas velocity at entry and at throat	Pressure drop and collection efficiency are studied as function of operating conditions like pressure ratio (ratio of operating pressure to suction pressure) and entrainment ratio (ratio of mass flow rates of entrained fluid to operating fluid)
Performance is studied with respect to design parameters like length, nozzle diameter, and throat aspect ratio (ratio of depth to width)	Performance is studied in terms of projection ratio(ratio of distance between nozzle end to commencement of throat) and area ratio (area of diffuser throat to area of nozzles)

2.3.1 Performance of high energy venturi scrubber

The performance of a venturi scrubber is measured by consideration of its collection efficiency and pressure drop. There are number of models documented in the literature to predict the venturi scrubber efficiency. These models are used in optimizing and designing new scrubbers or predicting the effect of changes in operating conditions and dimensional variables of existing equipments on their performance. Models proposed by Crowder et al. (1981) and Goel and Hollands (1977) have reported the limitations of complex mathematical expressions and the need to estimate physical properties data. A summary of models that are more realistic and have utility in prediction of pressure drop and collection efficiency are reviewed and presented in Table 2.6.

Mathematical models to predict pressure drop

Several attempts have been made to predict pressure drop across venturi scrubbers theoretically. However, none of these models accurately predict pressure drops for a wide range of operating conditions. The main models reported in the literature are:

- Calvert's Model (1970)
- Boll's model (1973)
- Annular flow model (AFM) (Viswanathan et al., 1985)
- Boundary layer growth model(BLM) (Azzopardi et al., 1991)
- Full boundary layer model (Sun et al., 2003)

Many researchers tried to predict pressure drop separately for atomization section, throat section and diffuser section. Almost all have presented their findings graphically on the plot either pressure or pressure drop vs. axial distance. The nature of plots is found to be almost similar qualitatively but they differ quantitatively. The pressure drop increases slowly till the entry of throat and then it suddenly rises in throat. In the diffuser some pressure is recovered and curve starts falling. Typical plots are presented in Figure 2.12, 2.13 and 2.14.

Table 2.6 : References for pressure drop and collection efficiency of HEVS

Sr. No	Reference	Type of scrubber studied	performance in terms of $\Delta p / \eta$	Parameters studied having effect on scrubber perf.	Property of Pollutant (particle diameters)	Ventury scrubber Geometry	Specific findings
1	Boll R.H. (1973) (1974)	R, H	$p, \Delta p, \eta$	$G, L/G, V_g, V_{gth}$	diameter of particle, drag coefficient, separation number	Diameter and length of throat	presented math. model that can be used to optimise, design and operating conditions in specific applications and to predict drop size.
2	Yung et al (1978)	HEVS	η	drop mdiameter	—	throat length	model to predict η .
3	Crowder, J.W. et al., (1981) (1982)	HEVS	$p, \Delta p$, angle of conv./div. throat length	$L, G, L/G, V_{gth}$	—	—	to optimise converging angle, throat length and diverging angle.
4	Crowder, J.W. et al., (1982)	HEVS/PA	η	—	—	contactor length	prediction of minimum contactor length
5	Ott Robert M. et al. (1987)	HEVS	η	$G, L/G$	diameter of particle	surface tension	new model presented
6	Monabbati et al. (1989)	HEVS	η	L, G	diameter of particle	—	new model presented
7	Viswanathan (1997)	HEVS/R	η	$G, L/G, V_g, V_{gth}$	diameter of particle	nozzel dia	The two-phase, two-component, annular flow unit was predicted.
8	R.A.Pulley (1997)	HEVS/PA/WA	$\eta, \Delta p$	$L, G, L/G, V_{gth}$	particle size	throat length	new model based on inertial mechanism.
9	Ananthanarayanan N V et al. (1998)	HEVS/R	η	$G, L/G, V_g$	diameter of particle	V_N/d , throat aspect ratio	$V_N 1.0-1.5 \times 10^{-3}$ offers maximum efficiency.
10	Viswanathan (1998)	HEVS/PA/R	$p, \Delta p$	$G, L/G, V_{gth}$, liq uid film	—	orifice diameter	a correlation has been developed to predict the liquid film thickness throughout the scrubber length.
11	Ananthanarayanan et al. (1999)	HEVS/PA/C	η	$G, L/G, V_{gth}$	diameter of particle	V_N	as V_N is independent of G , it is desirable to operate the scrubber in the range of 70-100 m/s to achieve maximum liquid utilization and collection efficiency
12	H. Sun et al. (2003)	HEVS/PA/WA	Δp	L, G	initial drop zize	orifice diameter	full boundary layer model has been presented.
13	Ravi G. et al. (2003)	HEVS/PA/R	η	$L/G, V_{gth}$	—	nozzle configuration	three-dimensional model for the collection η with the NSGA algorithm
14	Mohebbi et al. (2003)	orifice scrubber	$\eta, \Delta p$	particle diameter	—	—	particle-source-in-cell model proposed
15	Rahimi et al. (2004) and (2011)	HEVS/PA/R/C	Δp	$L, G, L/G, V_{gth}$	—	entering gas temperature/humidity	new concept of presentation of Δp in terms of number of throat velocity heads
16	Viswanathan et al. (2005)	HEVS/PA/R/C	$p, \Delta p$	$G, L/G, V_{gth}$	—	V_N , nozzel dia, throat aspect ratio	proposed-improved, ease, versatile and comprehensive algorithm to optimize scrubber performance which takes into account non-uniform liquid distribution
17	M.Taheri et al. (2008)	HEVS/PA/R	η	$L/G, V_{gth}$	diameter of particle	Diameter of throat	GA-ANN model is more efficient it has less AAPD
18	Silva et al. (2009)	HEVS/PA/WE/R /C	Δp	$L, G, L/G, V_{gth}$	—	—	model is inadequate for the prediction of pressure drop in the throat region
19	Nasseh et al. (2009)	HEVS/PA/R	Δp	$L/G, V_{gth}$	—	throat length	a neural network optimized by GA for predicting pressure drop in venturi scrubber.

Venturi type-HEVS-High energy Venturi Scrubber, EV-Ejector venturi scrubbere, R-Rectangular cross section, C-circular crosssection, PA-Pease-Antony type, WA-Wetted Approach G-gas velocity V_{gth} -Gas velocity at throat, L/G -Liquid to gas ratio (m^3/m^3), η -collection efficiency, R-Rectangular cross section, C-circular crosssection, V_N - Venturi number, AAPD - Average Absoulte Percent Deviation, GA = Genetic Algorithm, NSGA = Nondominated sorting genetic algorithm.

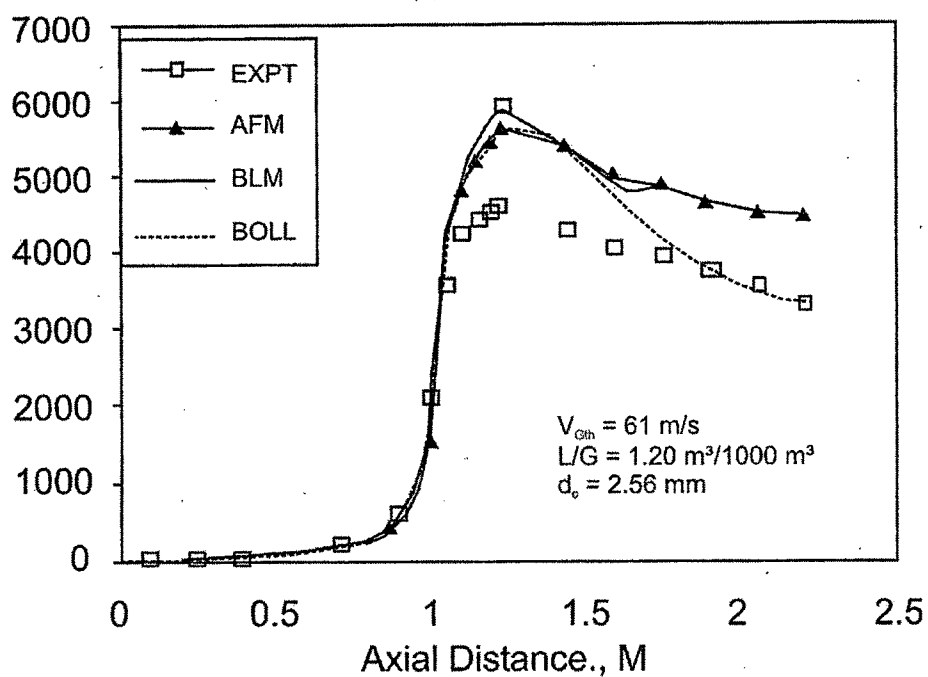


Figure 2.12 : Comparison of axial pressure drop predicted by different models with experimental data (Vishwanathan et al., 2005)

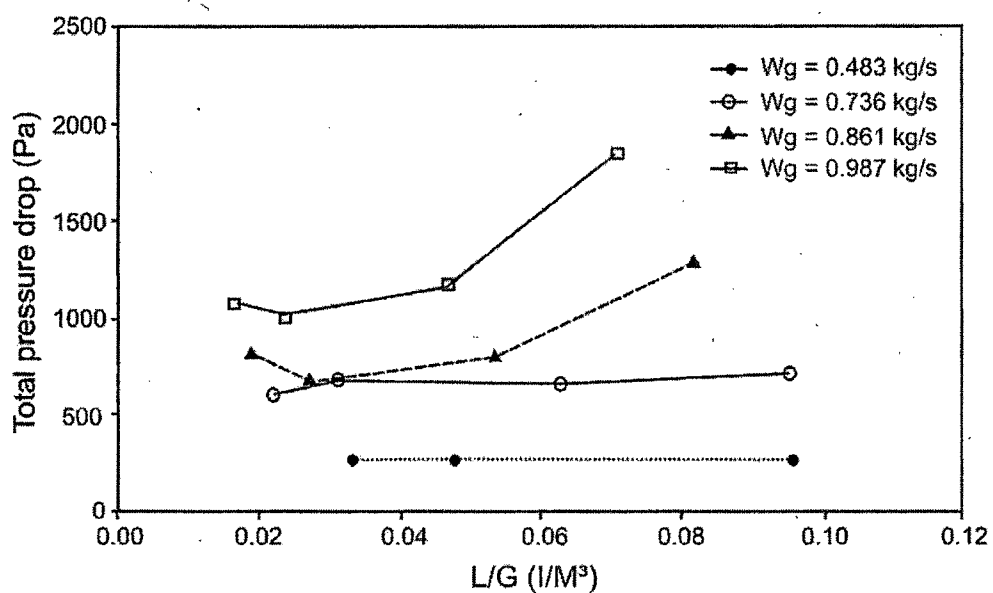


Figure 2.13 : Variation of the total pressure drop in the venturi with liquid to gas ratio and throat velocity. Liquid injected as a spray (Silva et al., 2009)

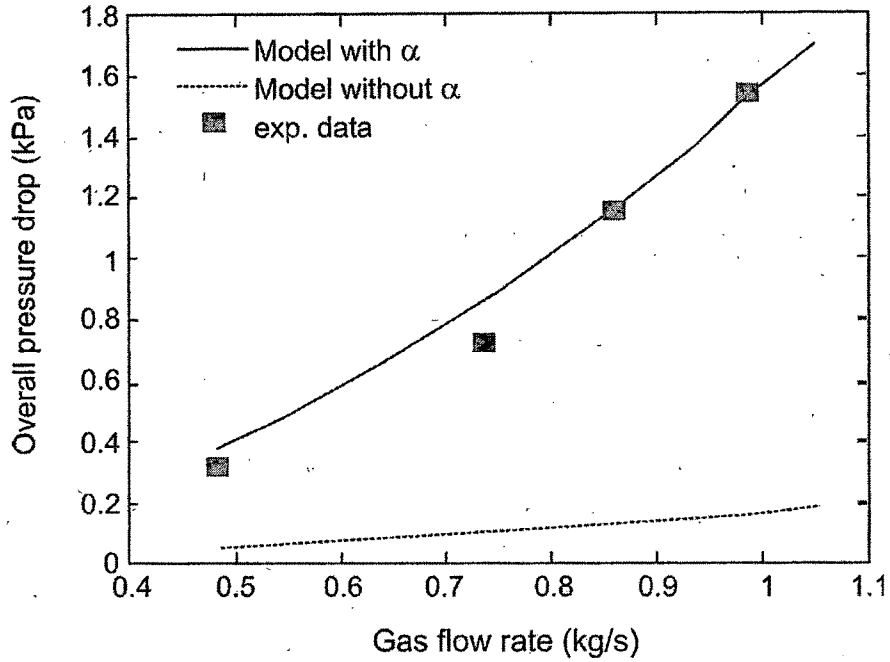


Figure 2.14 : Comparison of overall pressure drop predicted with and without correction factor α , experimental data of Silva et al. (2009) (Rahimi et al., 2011)

Collection efficiency

Jet ejector efficiency has been defined by researchers in different ways, like target efficiency, collection efficiency, overall efficiency and fractional efficiency (Mohebbi et al., 2003; Pulley 1997; Yung et al., 1977; Leith and Cooper, 1980; Boll 1973; Calvert 1970). The overall collection efficiency is defined as

- For particulate matter

$$\text{Collection efficiency} = \frac{\text{the mass of the removed particulate}}{\text{inlet of the mass of total flow of particulate matter}} \quad (2.14)$$

- For gaseous pollutant: Taheri et al. (2008) defined collection efficiency (the extent of absorption) as

$$\text{Collection efficiency (in\%)} = \frac{P_i - P_f}{P_i - P_e} \times 100 \quad (2.15)$$

where P_i , P_f and P_e are the initial, final, and equilibrium partial pressure of gaseous pollutant in mm of H_g , respectively

Collection efficiency have been reported with respect to gas/liquid ratio, gas and liquid flow rates , geometry of venturi scrubber like projection ratio P_R , length of throat, angle and length of convergent diffuser section and property of particulate/gas pollutants. Researchers have reported different empirical correlations to predict efficiency on the basis of different assumptions they have considered. The vast literature has been published on the subject. Table 2.6 is the summery of some of the earlier research. Typical graphical presentations are shown in Figure 2.15, 2.16, 2.17 and 2.18.

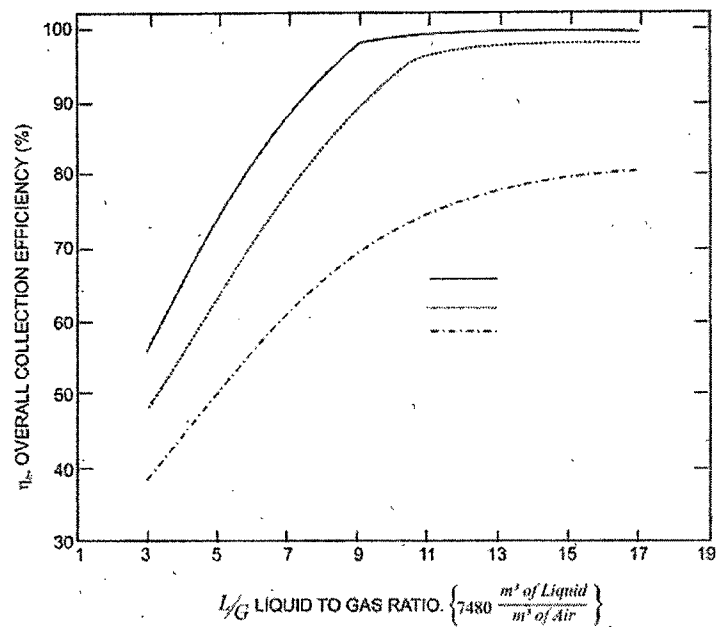


Figure 2.15 : Dependence of the overall collection efficiency of liquid gas ratio (Vishwanath et al., 1997).

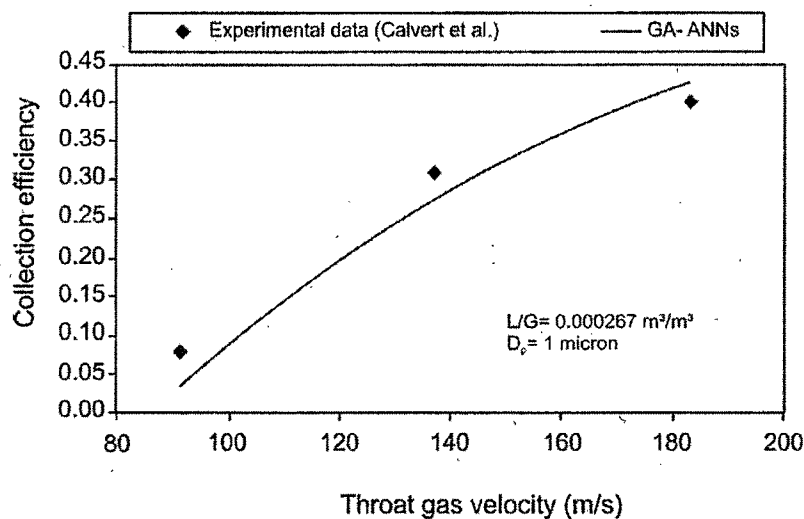


Figure 2.16 : The effect of throat gas velocity on the collection efficiency in venturi scrubber (GA-ANN no. 1). (Taheri et al., 2008)

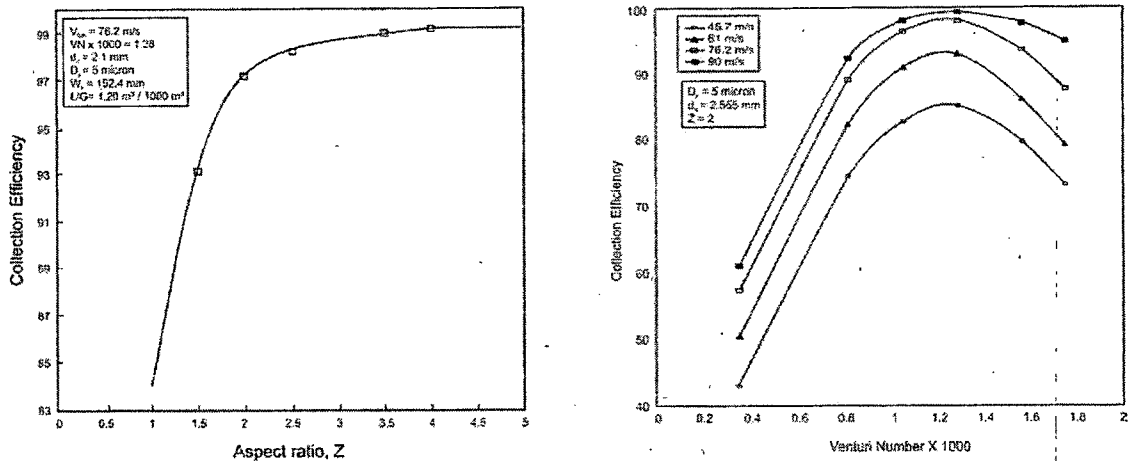


Figure 2.17 : Effect of variation in venturi number and aspect ratio on collection efficiency for a constant venturi number.

(Ananthanarayanan and Vishwanathan, 1998)

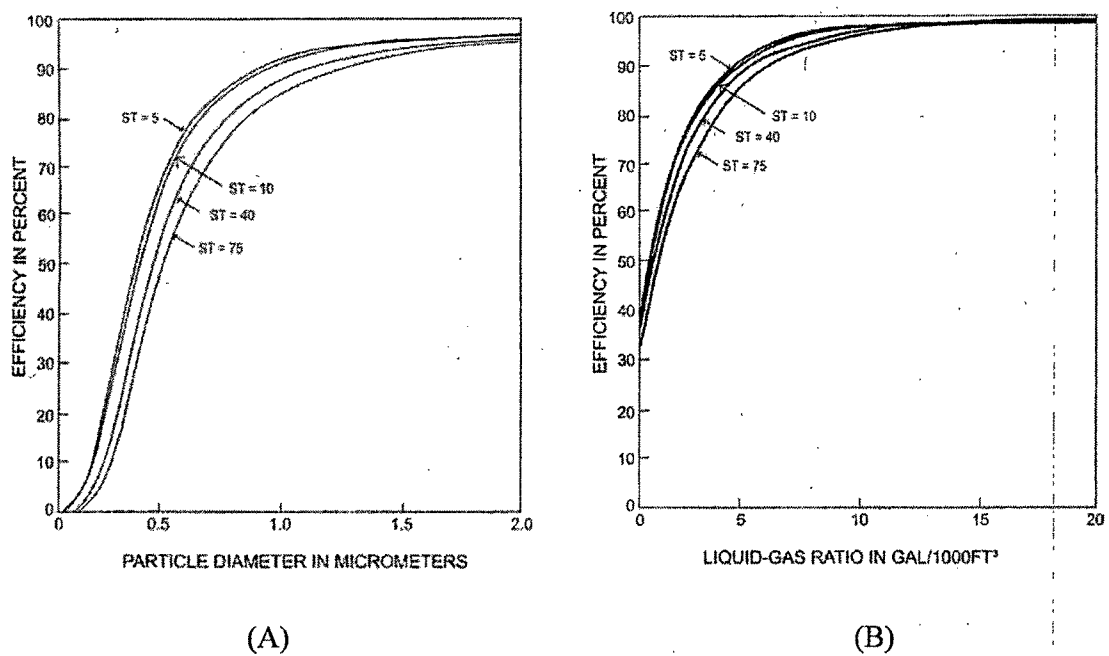


Figure 2.18 : Efficiency as a function of (A) particle diameter (B) liquid to gas ratio with liquid surface tension as a variable. (Ott et al., 1987)

Ott et al. (1987) developed a model studying the effect of surface tension on performance of venturi scrubber. They examined the effect of liquid surface tension on droplet size and on particle penetration into the droplet. (Figure 2.18A and B)

Economopoulou and Harrison (2007) developed graphical tools for estimating the overall collection efficiency of venturi scrubbers under the specified design and operating conditions

based on the well-established theoretical formulations of Calvert (1970) and Yung et al. (1978).

Taheri et al. (2010) simulated gas absorption in a venturi scrubber and developed a three-dimensional mathematical model, based on a non uniform droplet concentration distribution. They validated their model with the experimental data reported by Johnstone et al. (1954) and Wen and Fan, (1975) for SO_2 removal by using alkaline solution and H_2O . They used Lagrangian approach for water droplet movement. Yung et al. (1978) and Crowder et al. (1981) have developed mathematical models to study different parameters of high energy venturi scrubbers.

2.3.2 Jet ejectors

The application of jet ejector as vacuum producing device and as jet pump is well known (Gamisans et al., 2004; Govatos, 1981; Cunningham, 1974; Cunningham and Dopkin, 1974; Bonnington, 1956, 1960, 1964; Bonnington and King, 1972; Blenke et al., 1963; Kroll, 1947). With the fast growth of chemical process industry, their use as entraining and pumping device to handle corrosive fluids, slurries, fumes and dust laden gasses has increased. Their use as mass transfer equipment for liquid-liquid extraction, gas absorption, gas stripping, slurry reaction like hydrogenation, oxidation, chlorination, fermentation, etc. has increased. Due to increasing interest in the usage of jet ejectors, numbers of investigators have attempted to optimize their performance. (Das and Biswas, 2006; Gamisans et al., 2004; Gamisans et al., 2002; Dasappa et al., 1993; Mukharjee et al., 1988, 1981; Radhakrishnan and Mitra, 1984; Pal et al., 1980, 1975; Biswas et al., 1977, 1975; Acharjee et al., 1975; Singh et al., 1974; Bhat et al., 1972; Davis et al., 1967; Mitra and Roy, 1964; Mitra et al., 1963; Davis (1963).

Working of jet ejector

A jet ejector is a device in which suction, mixing and dispersion of secondary fluid is done by utilizing the kinetic energy of a motive (primary) fluid. Das and Biswas (2006) stated that when jet ejectors are used as a device for contacting gas-liquid, the secondary fluid may be dispersed by the shearing action of the high velocity motive fluid or the motive fluid itself may get dispersed when it is arrested by a secondary fluid. Figure 1.1 shows the typical

ejector system in which the jet of primary fluid issuing out of a nozzle creates a low pressure region around it. The pressure differential between the entry point of the secondary fluid and the nozzle tip provides the driving force for entrainment of the secondary fluid. Two principal flow regimes in ejectors are coaxial-flow and froth-flow. The coaxial-flow constitutes a central core of primary fluid with secondary fluid flowing in the annular region formed between the jet of primary liquid and ejector. Froth-flow regime is a co-current flow of fluids with one phase completely dispersed in the other. Witte (1969) termed the phenomenon of change from coaxial-flow to froth-flow as mixing shock. Here a part of the kinetic energy of the flow is dissipated in the shock creating the gas-liquid dispersion. The mixing shock results into generation of small bubbles and consequently creation of high interfacial area ($\sim 2000\text{m}^2/\text{m}^3$). Ejectors thus, give superior gas-liquid mass transfer rates and higher rates of reaction as compared to conventional gas-liquid contacting equipments like stirred tanks, bubble columns, packed columns, etc. Yadav and Patwardhan (2008) stated that there could be diverse objectives for ejector design depending on application as follows:

- (a) To get large entrainment of the secondary fluid.
- (b) To produce intense mixing between the two fluids.
- (c) To pump fluids from a region of low pressure to a region of high pressure.

Geometry of ejector

The significant parts of an ejector are (Refer Figure 2.19) primary fluid inlet, suction chamber, secondary fluid inlet, converging section, throat or mixing zone, diverging section or diffuser. The ejector may be specified by denoting nozzle diameter (D_N), throat diameter (D_T), diameter of suction chamber (D_S), length of throat (L_T), length of diffuser (L_D), distance between nozzle to commencement of throat (L_{TN}), angle of converging sections ($\theta_{convergent}$) and angle of diverging sections ($\theta_{divergent}$). Performance of the ejectors has been studied in terms of (a) area ratio ($A_R = A_T / A_N$), i.e., area of throat/area of nozzle, (b) throat aspect ratio (L_T / D_T), i.e., length of throat/diameter of throat, (c) projection ratio ($P_R = L_{TN} / D_T$), i.e., distance between nozzle tip to the commencement of throat / diameter of throat and (e) suction chamber area ratio [$A_S / A_N = (D_S^2 - D_N^2) / D_N^2$].

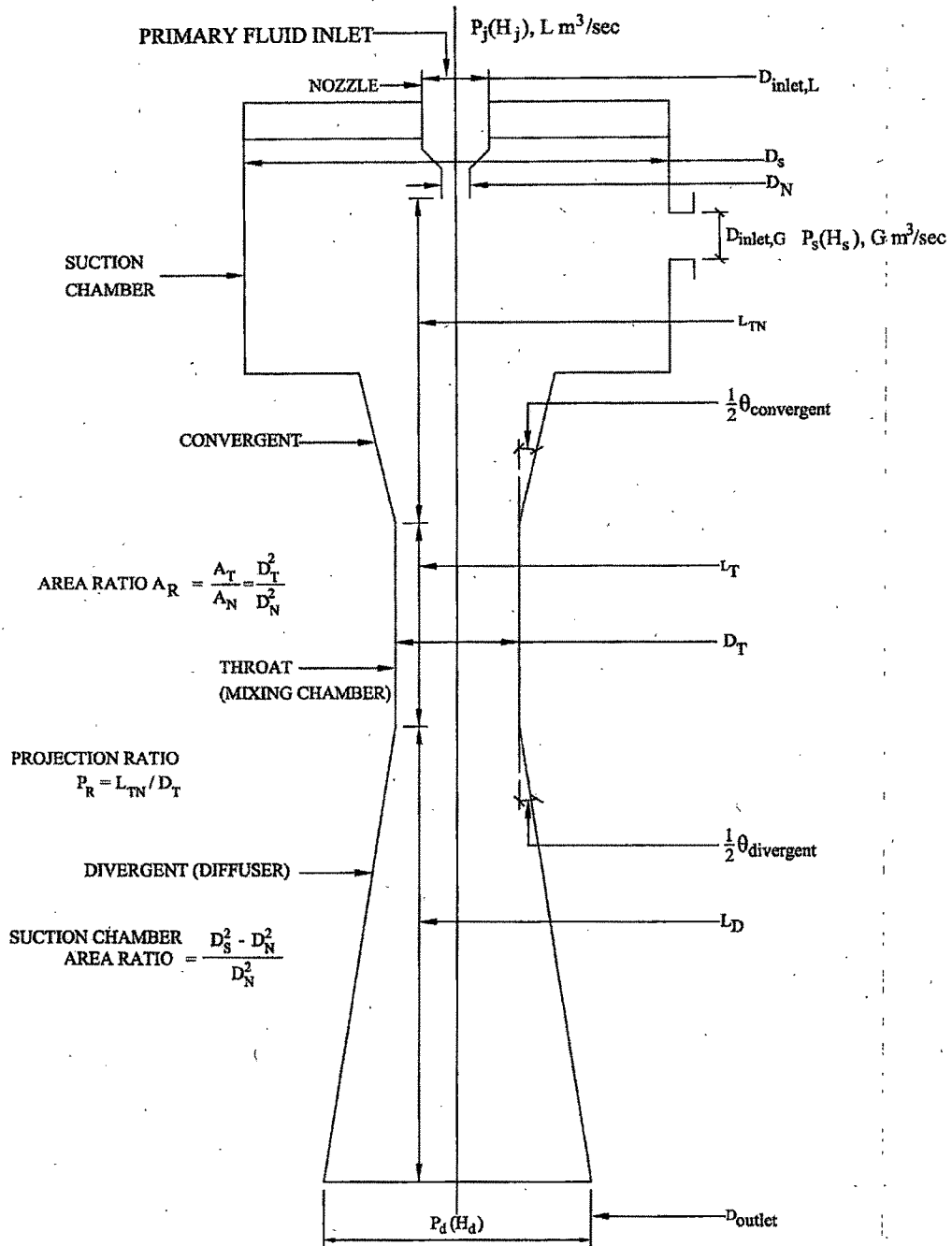


Figure 2.19 : Schematic diagram showing geometry of an ejector

Dutta and Raghavan (1987) studied and compared the performance of jet ejectors with and without venturi and throat. Similarly Gamisans et al. (2002) studied jet ejector without diffuser. Both of them concluded that the jet ejectors without diffuser or throat are less effective compared to ejector with them.

Many researchers have studied the mass transfer characteristics and performance of the jet ejectors followed by contactors, draft tube, packed column or bubble column (Li and Li, 2011; Rahman et al., 2010; Balamurugan et al., 2008, 2007; Utomo et al., 2008; Mandal, 2010; Mandal et al., 2005; 2004, 2003a, 2003b; Havelka et al., 2000, 1997; Dutta and Raghavan, 1987; Ogawa et al., 1983; Mitchell, 1981; Biswas et al., 1977). All have similar conclusion that there is less mass transfer coefficient in the extended portion compared to that in the ejector itself.

Effect of ejector geometry

Das and Biswas (2006) reported that the efficient functioning of an ejector depends on the design of the suction chamber, the mixing throat, the divergent diffuser and the forcing nozzle. Besides, the relative dimensions of the various parts of the ejector, the factors such as shape of the entrance to the parallel throat, angle of divergence and the projection ratio are also important factors to be considered.

Different investigators have studied the effect of geometry of jet ejector like area ratio, angle of convergence and divergence, projection ratio, shape of entry of convergent section, length of throat etc., Yadav and Patwardhan (2008) compiled dimensions of different components of ejectors studied by different investigators (See Table 2.7).

Area ratio (A_R)

The area ratio is defined as the ratio of area of throat (A_T) to area of the nozzle

$$A_R = \frac{A_T}{A_N} = \left(\frac{D_T}{D_N} \right)^2$$

Bonigton (1964) studied the effect of changing the diameter ratio i.e. ratio of nozzle diameter to throat diameter (D_N / D_T) instead of area ratio of the jet ejector performance. Acharjee et al. (1975), Singh et al. (1974), Bhat et al. (1972) and Mitra et al. (1963) studied the effect of area ratio on Mass ratio M_R (ratio of mass of driving fluid to the entrained fluid). It can be concluded from these studies that as the area ratio is increased the entrainment ratio also increases. But at the higher area ratio the increase in entrainment ratio becomes less. A typical correlation is shown in Figure 2.20.

**Table 2.7 : Geometrical parameters of ejectors used by deferent investigators
(Yadav and Patwardhan, 2008)**

References	Area ratio (D_T/D_N) ²	Entry to the throat	Angle of converging section (deg)	Throat aspect ratio (L_T/D_T)	Angle of diverging section (deg)	Projection ratio (L_{TN}/D_T)
Kroll (1947)	-	Well rounded	20-25	7	4--10	0.5--5
Davies et al. (1967)	22.6-247	Well rounded	--	7	10	1.9*
Bhat et al. (1972)	3.7-25.1	Conical	28	0	10	8.9
Cunningham and Dopkin (1974b)	2.2-6.5	Well rounded	--	12.3--32.4	4.0	3.0*
Acharjee et al. (1975)	5.4-50.4	Well rounded	--	8	10	2.0*
Biswas et al. (1975)	1.4--12.8	Well rounded	--	6	7	1.9*
Zahradnik et al. (1982)	33.8--113.8	Conical	--	0	6.4	--
Henzler (1983)	2.0--25.5	Well rounded	--	7.5	5	0.4--0.9*
Moresi et al. (1983)	1.5--3.5	Conical	17.35	1.8	9.5	--
Ben et al. (1984)	4.0	Conical	--	3.5	2.0	--
Bhutada and Pangarkar (1987)	1.8--10.2	Conical or bell- shaped	12	0--16	5.0	3.0*
Dutta & Raghwan (1987)	7.66-16	Conical	--	--	15	--
Mukherjee et al. (1988)	1--50.6	Well rounded	-	10.8	7	--
Panchal et al. (1991)	2.37 - 2.66	Conical	--	0	--	Pitch 1.1, 1.5, 2*
Kundu et al. (1994)	29.3--169.8	Conical	-	7	7	--
Kundu et al. (1995)	29.3--169.8	Well rounded	--	9.7	7	--
Havelka et al. (1997)	3.24	Conical	--	5--20	7	--
Agrawal (1999)	9.3	Well rounded	--	6	7	2
Fernandez (2001)	-	-	-	6	8	1.0
Cramers and Beenackers (2001)	2.1--9.0	Conical	--	2--10	3.0	--
Elgozali et al. (2002)	--	Conical	--	10	7	2.72
Gamisans et al. (2004)	--	Conical	--	0.5--1.3	--	--
Rusly et al. (2005)	2.5	Conical	10	5.0	7	5.0
Mandal et al. (2005a)	10.0	Well rounded	--	9.7	9.1	--
Mandal et al. (2005b)	5.6--14.4	Well rounded	--	9.7	9.1	--
Majumder et al. (2005)	7.4--22.5	Well rounded	--	9.6	7	--
Li and Christofides (2005)	--	Conical	12	1.1	2	2.17
Das and Biswas (2006)	15.5--59.5	--	--	7.76	8.6	--
Sriveerakul et al. (2007)	5.6--10.0	Well rounded.	--	1--6	10	1.1-6.8
Mukherjee et al. (2007)	9.9 - 39	Well rounded	--	6.5	7	--
Balamurugam et al. (2008)	1.1 - 6.45	Well rounded	--	0 - 4	--	2 - 4
Utomo et al. (2008)	6.69	--	--	4-10	3.5	--
Appusamy et al. (2008)	4.48 - 40	Well rounded	--	2.95 - 7	--	--
Yadav & Patwardhan (2008)	4	Well rounded	2.5 - 9	0	4.85	0 - 14.5
Raghuram (2009)	1	--	--	7	9	--
Rahman (2010)	6.76 - 18.7	Conical	--	4.8	--	--

*Indicate the optimum value suggested by the investigator

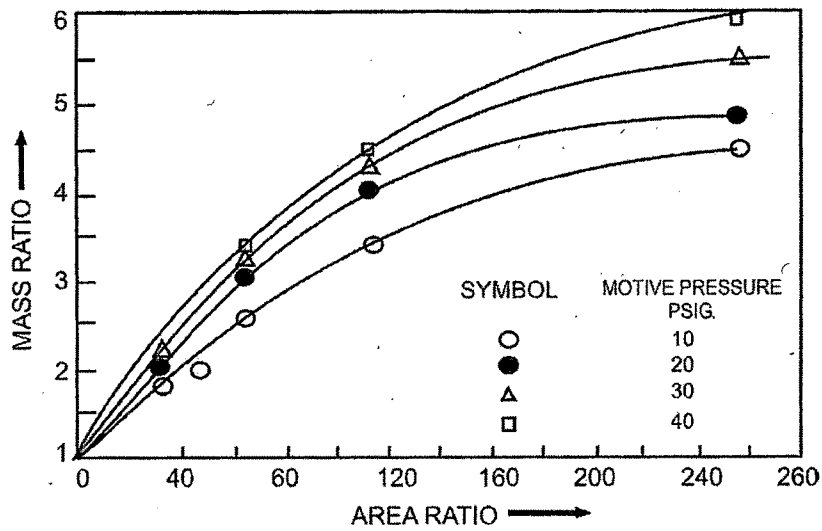


**Figure 2.20 : Effect of area ratio on mass ratio for water-water system
(Singh et al., 1974)**

Projection ratio

The projection ratio (P_R) is defined as the ratio of the distance between the injecting nozzle to the commencement of throat (L_{TN}) to diameter of throat (D_T)

$$P_R = \frac{L_{TN}}{D_T} \quad (2.16)$$

A typical plot of M_R vs. P_R is presented in Figure 2.21. It is observed that as P_R rises the entrainment ratio is not much effected but at definite value of P_R , the M_R , rises suddenly and

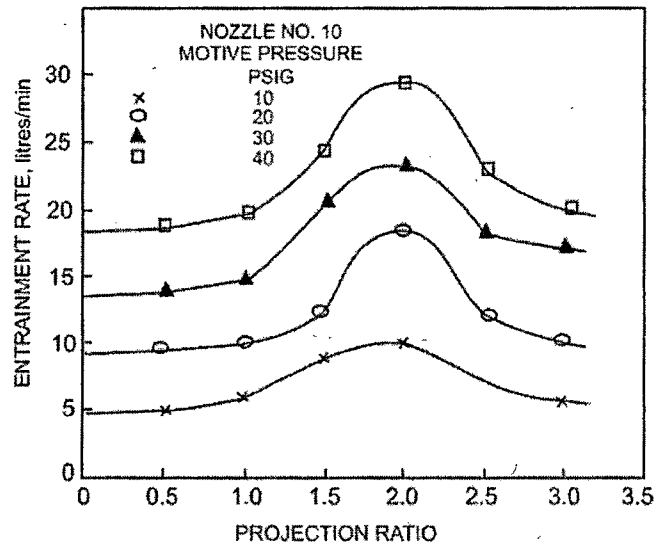


**Figure 2.21 : Variation of entrainment of air with projection ratio of water-air system
(Acharjee et al. 1975)**

again falls to previous value. Thus P_R at which it draws maximum entrained fluid is considered to be optimum. Biswas et al. (1975), Acharjee et al. (1975) and Devis et al. (1967) had similarly observed that at P_R around 2.10 is optimum. Singh et al. (1974) in their research study observed optimum P_R as around 0.5. It has been suggested that the optimum P_R is influenced by geometry of entrance to the mixing tube. Table 2.7 shows that the optimum value of P_R suggested by the different investigators is different. Yadav et al., (2008) utilized computational fluid dynamics (CFD) modeling to study the role of P_R , angle of converging section and diameter of suction chamber. They studied the effect of P_R (0, 2.5, 5, 10 and 14.5) on entrainment, pressure profile along the axis of ejector and power efficiency. They concluded that the rate of entrainment and power efficiency increases as the projection ratio increases that is because of the fact when one increases the P_R it leads to the reduction in the generation of radial flow. However beyond $P_R > 5$ negligible amount of radial flow is generated and hence the rate of entrainment and energy efficiency remain constant. Hence it may be considered that the optimum projection ratio is 5 (Figure 2.22).

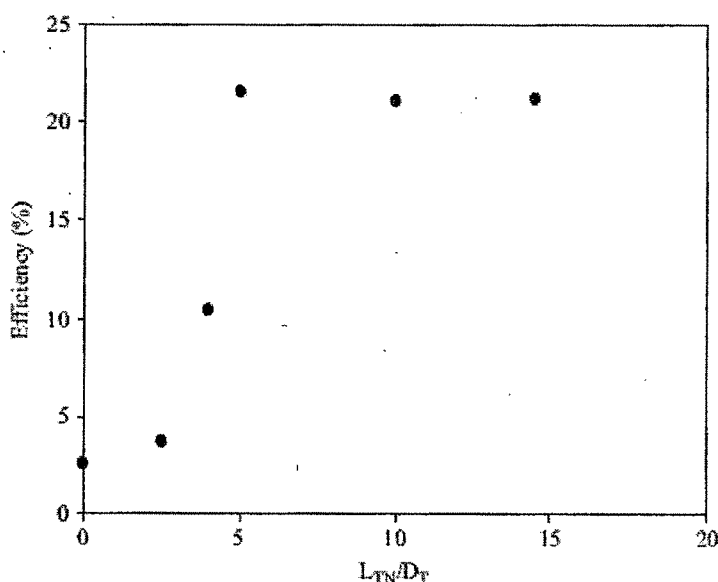


Figure 2.22 : Effect of projection ratio (L_{TN}/D_T) on energy efficiency (Yadav and Patwardhan, 2008)

Diameter of suction chamber (D_S)

Though cross sectional area of the suction chamber is important parameter which effects the performance of venturi, it has not been given the necessary attention. Yadav and Patwardhan (2008) studied the effect of diameter of suction chamber. To study the effect of suction chamber diameter they defined suction chamber area *ratio* (A_S / A_N) as

$$\text{Suction chamber Area ratio} = \left(\frac{A_S}{A_N} \right) = \frac{D_S^2 - D_N^2}{D_N^2} \quad (2.17)$$

They concluded that maximum power efficiency (20 to 25%) is obtained for $(D_S^2 - D_N^2)/D_N^2 = 6.6$ and for $(D_S^2 - D_N^2)/D_N^2 > 13.6$ it remain constant. (Refer Figure 2.23)

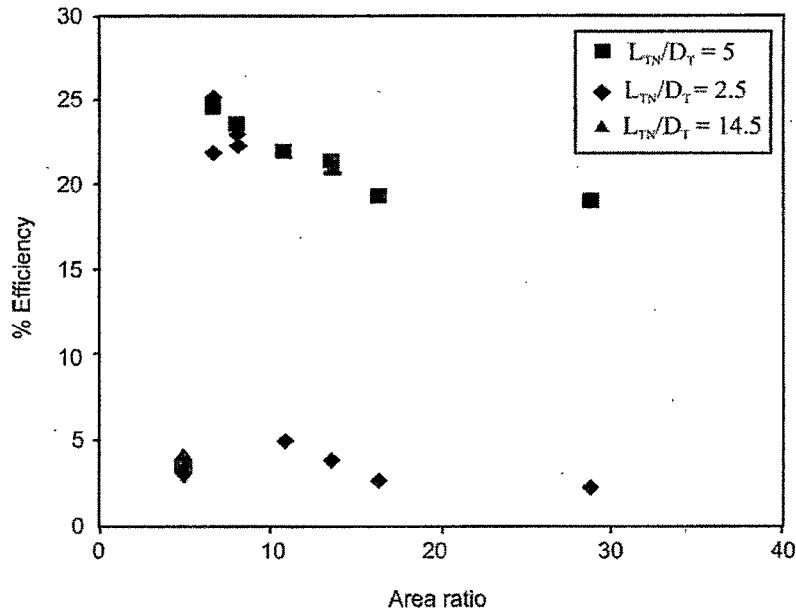


Figure 2.23 : Effect of area ratio $(D_S^2 - D_N^2)/(D_N^2)$ on efficiency of ejectors for different values of projection ratio (Yadav and Patwardhan, 2008)

Effect of angle of convergent section and divergent section

It can be seen from Table 2.7 that numbers of investigators have worked to find optimum angle of convergence and divergence. Yadav and Patwardhan (2008) studied the effect of angle of convergence on entrainment and efficiency. In Figure 2.24 entrainment for different angles: 2.5°, 10°, 30° and 90° has been shown. It can be seen that the rate of entrainment is low for $\theta = 2.5^\circ$. It increases with increase in θ and attains a maximum value for $\theta = 10^\circ$. Further increase in θ results in decrease in the rate of entrainment of the secondary fluid. Similarly their study shows that the largest pressure driving force is generated for $\theta = 10^\circ$ and it results in the highest entrainment for this case. With increase in θ beyond 10° the pressure driving force was observed to reduce and it results in decrease in the rate of entrainment. They also showed that highest efficiency is obtained at $\theta = 10^\circ$ and larger values of θ results in poor energy efficiency. Thus, they suggested for obtaining maximum entrainment the angle of convergent may be kept between 5° – 15° . The angle of divergent section has been kept between 7° to maximum 10° by many of the investigators.

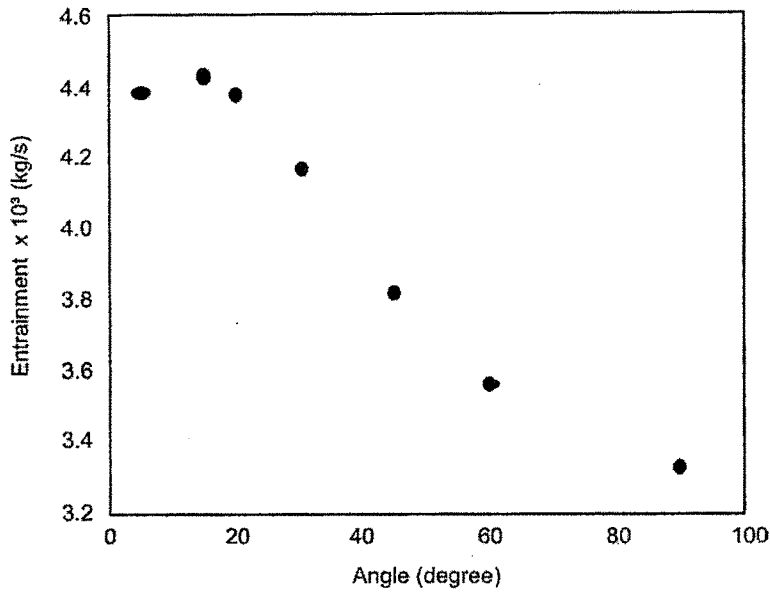


Figure 2.24 : Effect of angle of converging section (θ) on rate of entrainment (Yadav and Patwardhan, 2008)

Mathematical models

Utomo et al. (2008) developed three dimensional CFD model to investigate mass transfer characteristics. They varied the gas-liquid flow ratio in the range of 0.2 to 1.2 and the length to diameter ratio of mixing tube (L_{TN}/D_{MT}) from 4 to 10. Their CFD studies show that at $L_{TN}/D_M = 5.5$, the volumetric mass transfer coefficient increases with respect to gas flow rate. They observed that at $L_{TN}/D_M = 4$, the graph of volumetric mass transfer coefficient vs gas-liquid flow rate ratio reaches the maximum at gas-liquid flow rate ratio of 0.6. A remarkable observation in their study was that volumetric mass transfer coefficient decreases with the increase of mixing tube length. They validated results obtained from CFD with the experimental result (configuration of ejector has a mixing tube diameter of 22 mm and diffuser outlet diameter of 40 mm, diffuser angle of 3.5 and a draft tube length of 100 mm.). The mixing tube lengths are varied between 88 and 220 mm with the nozzle diameter of 8.5 mm.

Kandakure et al. (2005) developed a CFD model to understand the hydrodynamic characteristics of ejectors. They varied the value of the slip velocity between the phases for validation keeping nozzle velocity constant (at different height to diameter ratio of throat) to validate the model. They found that when the slip velocity is made 13% of the axial water velocity, it matches the experimental data very well. They found that the predicted air

entrainment is the maximum for the ejector with height to diameter ratio of throat equal to zero and the area ratio of 4. They justified that the CFD simulations eliminate all such empiricism.

Kim et al. (2007) studied rectangular bubble column ($0.22 \times 0.26 \times 1.3m$) with a horizontal flow ejector. They investigated the effect of the ejector geometry i.e. nozzle diameter and mixing chamber diameter and the operating conditions like liquid flow rate and liquid level in rectangular column, on the hydrodynamic characteristics. They established that the gas holdup increases with increasing liquid flow rate and decreases with increasing level of liquid in the rectangular column. They applied the multiphase CFD simulation with the mixture model and found that the gas entrainment rate increases with increasing liquid flow rate contrary to this the gas suction rate decreases with increasing nozzle diameter and the liquid level in the rectangular column. The predicted values obtained from CFD simulation were compared with the experimental data, which were well matching.

Li and Li (2011) investigated the entrainment behavior and performance of gas-liquid ejectors using different software and computational technique like Computational Fluid Dynamics (CFD) and validated with experimental data over a wide range of operating conditions for ejector with different configurations.

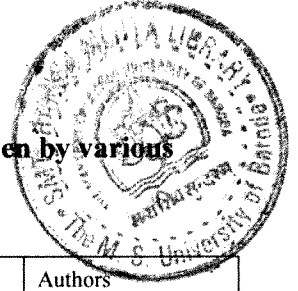
2.3.3 Parameters other than geometry of the ejector

Many investigators (Gamisans et al., 2004, Gamisans et al., 2002, Ben. et al.1984; Bhutada, and Pangarkar, 1987; Acharjee et al., 1975, Singh et al., 1974; Bhat et al., 1972; Davis et al., 1967; Mitra and Roy 1964; and Mitra et al., 1963) studied effect of mass ratio (M_R) as a function of motive pressure, suction pressure, separator pressure, pressure drop, A_R , P_R , Reynold's number, Euler's number etc. Some of investigators (Mitra et al., 1963; Bonington 1964) studied the effect of head ratio on ejector performance, head ratio is defined as:

$$\text{Head ratio} = \frac{\text{Head generated by suction fluid}}{\text{Head lost by driving fluid}} = \frac{H_D - H_s}{H_j - H_s} \quad (2.18)$$

where H_D = pressure head at discharge of ejector, m; H_s = pressure head at suction of ejector, m; and H_j = operating pressure, m. The empirical equations to predict mass ratio (M_R) from dimensionless analysis given by various authors are summarized in Table 2.7a. Similarly table 2.7b summarizes mass ratio (M_R) correlations from theoretical analysis given by various authors.

Table 2.7a : Mass ratio correlations from dimensionless analysis given by various authors (Balamurugan et al. (2007))



Primary fluid	Secondary fluid	Geometry and range investigated	Mass ratio correlation	Authors
Air	Water	Flow—upward: $D_N = 0.00808\text{--}0.002676\text{ m}$, $D_T = 0.0127\text{ m}$, $H_T = 0.0889\text{ m}$, $(D_N/D_T) = 0.009\text{--}0.2107$, $D_C = 0.0635\text{ m}$, $H_C = 1.219\text{ m}$	$M_r = k \left(\frac{\mu m}{D_N \rho_m U_m} \right)^{0.76} (A_r)^{0.4}$ $\left(\frac{g \mu_e^4}{\rho_e \sigma_e^3} \right)^{-0.04} \left(\frac{\rho_e - \rho}{\rho_e} \right)^{0.63}$	Davies et al. (1967)
Water, glycerin, kerosene	Air	Flow—horizontal: $D_N = 0.0019\text{--}0.00449\text{ m}$, $D_T = 0.00925\text{ m}$, $D_N/D_T = 0.2\text{--}0.48$, $H_T = 0$, $D_C = 0.0254\text{ m}$, $H_C = 1.1\text{ m}$	$M_r = 8.5 \times 10^{-2} \left(\frac{\Delta P}{\rho_e U_e^2} \right)^{-0.3}$ $(A_r)^{0.46} \left(\frac{g \mu_m^4}{\rho_m \sigma_m^3} \right)^{-0.02}$	Bhat et al. (1972)
Water, glycerin, kerosene	Air	Flow—upward: $D_N = 0.00178\text{--}0.0055\text{ m}$, $D_T = 0.0127\text{ m}$, $H_T = 0.1016\text{ m}$, $D_N/D_T = 0.14\text{--}0.433$	$M_r = 5.2 \times 10^{-4} \left(\frac{\Delta P}{\rho_e U_e^2} \right)^{-0.305}$ $(A_r)^{0.68} \left(\frac{g \mu_m^4}{\rho_m \sigma_m^3} \right)^{-0.305}$	Acharjee et al. (1975)
Water, mono ethylene glycol	Air	Flow—downward: $D_N = 0.0025\text{ m}$, $D_T = 0.005\text{ m}$, $H_T = 0.0175$, $D_N/D_T = 0.5$, $H_C = 1\text{ m}$, $D_C = 0.01\text{ m}$	$M_r = 43.86 \times 10^{-3} \left(\frac{\Delta P}{\rho_e U_e^2} \right)^{-0.38}$ $\left(\frac{g \mu_m^4}{\rho_m \sigma_m^3} \right)^{-0.01}$	Ben et al. (1984)
Water	Air	Flow—downward: $D_N = 0.0045, 0.0065\text{ m}$, $D_T = 0.018\text{ m}$, $D_C = 0.040\text{ m}$	$M_r = 2.4 \times 10^{-3} \left(\frac{\Delta P}{\rho_e U_e^2} \right)^{-0.82}$ $\left(\frac{g \mu_m^4}{\rho_m \sigma_m^3} \right)^{-0.01}$	Dutta & Raghvan (1987)
Water	Air	Flow—downward: $D_N = 0.005, 0.008, 0.01, 0.012\text{ m}$, $D_T = 0.016, 0.0159\text{ m}$, $D_N/D_T = 1.6\text{--}3.2$	$M_r = x \left(\frac{\Delta P}{\rho_e U_e^2} \right)^y (A_r)^z; x$ $= 5.58 \times 10^{-4} \text{ to } 9.67 \times 10^{-4};$ $y = -0.135 \text{ to } -0.202; z$ $= 0.07\text{--}0.224$	Bhutada & Pangarkar (1987)
Water	Water	Flow—horizontal: $D_N = 0.00159, 0.00238, 0.003175, 0.00397, 0.00437\text{ m}$ $D_T = 0.025\text{ m}$ $D_N/D_T = 0.0625 \text{ to } 0.17$	$M_R = 3.2 \times 10^{-2} (Re_f)^{0.25}$ $(A_R)^{0.70} ((g_c \Delta p) / (\rho_s u_s^2))^{-0.38}$	Singh et al. (1974)

Table 2.7b : Mass ratio correlations from theoretical analysis given by various authors

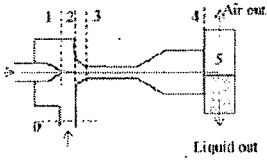
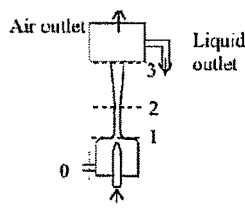
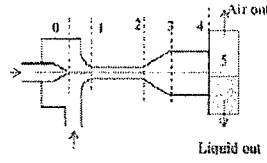
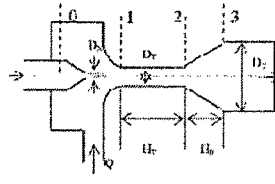
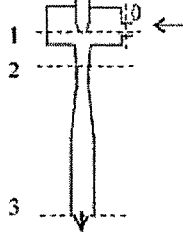
Geometry and range investigated	Geometry and the locations where the energy and momentum balance were taken	Correlation and remarks on loss coefficient	Authors
Flow—horizontal: $D_N = 0.0019-0.00449$, $D_T = 0.00925$, $D_N/D_T = 0.2-0.48$, $H_T = 0$, $D_C = 0.0254$, $H_C = 1.1$. Primary fluid—water, glycerine and kerosene Secondary fluid—air maximum $L/G = 60$		$M_r^2 \rho_r \left[-\gamma_2^2 + \frac{2\gamma_1 A_r}{(A_r - 1)} + 2(\gamma_1 - 1) \right. \\ \left. \left(\frac{\gamma_3}{\gamma_3 - 1} \right) \left(\gamma_3 - \frac{A_r}{A_r - 1} \right) - \gamma_1^2 \right] \\ - M_r \gamma_1^2 (\rho_r + 1) - (\beta + K') A_r^2 + 2\gamma_1 A_r \\ - (\gamma_1^2 + \gamma_2^2) = 0$ <p>All the losses are clubbed as loss factor K' and values of K' were fitted using experimental results</p> <p>K' was empirically fitted to β and A_r</p> $K' = -\beta - 0.0123 A_r + 0.116$ <p>Each area ratio has different K' and the value ranges from 0.01 to 0.06</p>	Bhat et al. (1972)
Flow—upward: $D_N = 0.00178-0.0055$, $D_T = 0.0127$, $H_T = 0.1016$, $D_N/D_T = 0.14-0.433$ Primary fluid Water, glycerin, kerosene Secondary fluid—air		$M_r^2 \rho_r \left[\gamma_a^2 + \frac{A_r(A_r - 2)}{(A_r - 1)^2} - 1 \right] \\ - M_r (\rho_r + 1) + 2A_r \\ - (K' + \beta) A_r^2 - 1 = 0$ <p>All the losses are clubbed as loss factor K' and was fitted to match the experimental values</p> $K' = -0.82\beta + \frac{1.52}{0.95A_r}$ <p>Each area ratio has different K' and value ranges from 0.01 to 0.28</p>	Acharjee et al. (1975)
Flow—horizontal: $D_N = 0.00278-0.00798$, $D_T = 0.01$, $H_T = 0.06$, $D_N/D_T = 0.278-0.798$, $D_C = 0.0254$, Primary fluid—water, nacl, acetone—water mixture (30%) and glycerol (30%) Secondary fluid—air Maximum $L/G = 14$		<p>Total suction was obtained for single phase from loss at each section</p> <p>Total suction created partially utilized for entrainment and dispersion</p> $M_r^2 = \frac{K_s f_s^n \rho_e}{\rho_m} \left[K' \gamma_3^2 + K_1 \gamma_2^2 + \frac{4f_1 H_T}{D_T} + \frac{4f_2 H_{CY_2}}{D_C} + (1 + K_D)(1 - \gamma_2)^2 \right]$ <p>K_s and n are fitted from experimental data</p>	Biswas and Mitra (1981)
Flow—horizontal: review of existing data, single phase		<p>Total loss coefficient = 1 - diffuser efficiency + loss coefficient of throat</p> $P_3 - P_{OS} = \frac{\rho_m}{2} U_m^2 \left[\frac{2}{A_r} \left(\frac{M_r^2 \rho_r}{A_r - 1} + 1 \right) - \frac{M_r^2 \rho_r}{(A_r - 1)^2} (1 - K_N) - \frac{(1 + M_r)(M_r \rho_r + 1)}{A_r^2} (1 + K_I) \right]$ <p>K_I and K_N were obtained from experimental data of previous authors also single loss coefficient was proposed. Value of K' ranges from 0.21 to 0.34</p>	Henzer (1983)

Table 2.7b continued

<p>Flow—downward: $D_N = 0.0025$, $D_T = 0.005$, $H_T = 0.0175$, $D_N/D_T = 0.5$, $H_C = 1$, $D_C = 0.01$</p> <p>Primary fluid—water, mono ethylene glycol Secondary fluid—air</p> <p>Maximum L/G = 15</p>		$M_r^2 \rho_r \left[\gamma^2 \frac{A_r'}{A_r} + \frac{A_r (A_r' - 2)}{(A_r' - 1)^2} \right] + 2A_r + \frac{1 + M_r}{M_r \rho_r (1 + \epsilon) + 1} + [2A_r^2 Fr - M_r \rho_r (1 + \epsilon) + 1] - (K'' + \beta) A_r^2 = 0$ $K' = -1.11\beta + 0.445$ <p>All the losses are clubbed as loss factor K' and was fitted with experimental values. Values of K' ranges from 3–7</p>	<p>Ben et al. (1984)</p>
---	---	--	--------------------------

Bonington (1964) published a plot of power efficiency vs head ratio with diameter ratio as parameter. As per their co relation the maximum efficiency achieved is around 33% at head ratio 4 and diameter ratio (ratio of diameter of nozzle to throat diameter) 0.52. Similar studies have also been done by Yadav and Patwardhan (2008), Gamisans et al. (2004), Cunningham (1974) and Blenke et al. (1963).

Yadav and Patwardhan (2008) defined Energy efficiency of ejector as

$$\% \eta = \frac{\text{power imparted to the secondary fluid}}{\text{power of fluid coming out of the nozzle}} \times 100 \quad (2.20)$$

Where

$$\text{Power of fluid coming out of the nozzle} = (\text{Power})_P = \frac{\pi}{8} \rho_P D_N^2 V_j^2 \quad (2.21)$$

and

$$\text{Power imparted to the secondary fluid} = (\text{Power})_S = (P_{\text{outlet}} - P_{\text{throat}}) Q_S \quad (2.22)$$

where P_{outlet} is absolute pressure at diffuser outlet, Pa; P_{throat} is absolute pressure at throat, Pa; Q_S flowrate of secondary fluid, m^3/s ; ρ_P is density of the primary fluid, kg/m^3 ; D_N , diameter of nozzle, m; V_j , velocity of primary fluid at outlet of nozzle.

2.4 Gas absorption in jet ejector

In any absorption process, whether followed by a chemical reaction or not the gas must first be dissolved in the liquid. Thus, gas liquid mass transfer is one of the most fundamental steps in determining the absorption rate or the overall reaction rate. (Charpentier, 1976)

There is scanty literature available on the study of mass transfer in jet ejector. The rate of mass transfer is expressed by studying interfacial area between two phases, liquid side mass transfer coefficient k_L and gas side mass transfer coefficient k_G (Shabani, 2010). There are different factors which influence the value of a , k_L and k_G .

Physico-chemical factors

Solubility of solute in liquid phase and its diffusivity, concentration of reacting reagent in the liquid, reaction rate constant, reaction equilibrium constant, viscosity and density of liquid, etc. are important physico-chemical factors. Danckwerts (1967) showed the effect of change in temperature at the surface (resulting due to the heat of absorption and the heat of reaction) on change in concentration of the product of the reaction at the surface and depletion of reactant dissolved in liquid at the surface (in case of pseudo-first order reaction).

Shabani et al. (2010) has been reported that mass transfer rate is a severe function of solution concentration and effective interfacial area.

Hydrodynamic factors

Gas flow rate, liquid flow rate and gas to liquid flow ratio are main hydrodynamic factors which affect the rate of absorption. Laurent (1978) established the hydrodynamic characteristics in the jet ejector. They studied the influence of the gas and liquid flow rates and the diameter of the ejector on the rate of mass transfer.

2.4.1 Methods of determination of interfacial area

There are mainly three methods used to determine the interfacial area that are reported in the literature:

1. Measuring the drop size and drop size distribution
2. Photographic method
3. Chemical method

In the present study the chemical method for measuring interfacial area is used. In this method, gas-liquid chemical reaction is utilized to measure the interfacial area and volumetric mass transfer coefficient. One of reacting component (known as solute) like CO_2 , SO_2 , O_2 and Cl_2 from gas phase is absorbed in liquid phase which contains another reactant like ammonia, sodium carbonate, dithionite, cuprous chloride, caustic soda or sodium sulfite. Oyevaar and Westerterp (1989) concluded that the error in interfacial area measured by chemical method is less than 10% and 20% for mechanically agitated reactor and bubble column respectively, if the conversion is less than 99%. Raghuram (2009) used photographic method to determine interfacial area and bubble diameter.

Weisweiler and Rosch (1978) studied interfacial area and bubble size distribution in jet reactors using $CO_2/N_2 - NaOH$ system. They used chemical method to investigate interfacial area.

2.4.2 Determination of interfacial area by chemical method

According to the study of Dehkordi and Savari (2011), the theory of gas absorption accompanied by a chemical reaction explained by Danckwerts (1970, 1968), has been widely used to evaluate the volumetric liquid-side mass-transfer coefficient $k_L a$ and the specific interfacial area a in various gas-liquid contactors.

Consider a chemical reaction between gas component A and a component B in liquid phase. This reaction may be written as follow:



If the reaction is irreversible of the m^{th} order in A and n^{th} order in B , the local rate of reaction per unit volume may be expressed by

$$-r_A = k_{mn}[A]^m[B]^n \quad (2.24)$$

where $[A]$ and $[B]$ are the local concentrations of A and B respectively. Doraiswamy and Sharma (1984) stated that if reaction satisfies

$$\sqrt{M} = \frac{\left(\frac{2}{m+1} D_A k_{mn} [A^*]^{m-1} [B_0]^n \right)^{1/2}}{k_L} \ll 1 \quad (2.25)$$

and

$$\sqrt{M} = \frac{\left(\frac{2}{m+1} D_A k_{mm} [A^*]^{m-1} [B_0]^n\right)^{1/2}}{k_L} \ll \frac{1}{3} \frac{[B_0]}{[A^*]} \quad (2.26)$$

where $[A^*]$, $[B_0]$, D_A , and k_L are the solubility of gas in the aqueous solution, initial concentration of reactant B, molecular diffusivity of A in the aqueous solution, and the mass-transfer coefficient, respectively.

Then the reaction between A and B occur entirely in the film, and the concentration of B at the interface is practically the same as that in the bulk of the liquid phase. Here \sqrt{M} represents the ratio of the amount of A reacting in the film to that of amount A reacting in the bulk. If the reaction is pseudo- m^{th} order in A and the rate of absorption of component A per unit volume of the reactor can be expressed by

$$R_A a = a [A^*] \left(\frac{2}{m+1} D_A k_{mm} [A^*]^{m-1} [B_0]^n \right)^{\frac{1}{2}} \quad (2.27)$$

Here, it may be interpreted that under these condition the rate of absorption is independent of k_L or the hydrodynamic conditions. So it means that if reaction is fast pseudo- m^{th} order, then by having the knowledge of solubility of the gas ($[A^*]$), the molecular diffusivity of the gas component dissolved in the liquid phase (D_A) and the kinetic parameters of the reaction (i.e., n, m and k_{mm}), specific interfacial area a can be evaluated by determining experimentally rate of absorption of A per unit volume of the reactor ($R_A a$).

Jhaveri and Sharma (1968) compared the work of different researchers who studied absorption accompanied by pseudo m^{th} order reaction to evaluate the effective interfacial area, a , as a function of the liquid flow rate in a laboratory packed column. Oxygen was absorbed in aqueous solutions of cuprous chloride and sodium dithionite. Isobutylene was absorbed in an aqueous solution of sulfuric acid. There is a good agreement among the values of a obtained by using different systems. The value of a appears to be a unique function of the liquid flow rate in the range of liquid properties covered in their investigation (*ionic strength* 1 to 34.5 g ion/l, viscosity 1 to 9 cP). They further concluded that the effective interfacial area remains practically the same irrespective of the reacting species and the kinetics of the reaction. Similarly Gemisans et al. (2002) studied different arrangement of jet ejector like single stage, two stages with and without secondary jet and without throat using absorption of SO_2 and NH_3 from the gas into $NaOH$ and H_2SO_4 solutions respectively. They studied the effect of variation in solute concentration, air flow rate and absorbing solution

flow rate. They observed that the liquid flow rate have strong influence on a where as the solute concentration and gas flow rate have slight influence. These results are in consonance with the observations of Jhaveri and Sharma (1968). They have also concluded that there was considerable improvement in absorption efficiency in case of two stage jet ejector having only one jet, but there was increased energy consumption. Shabani et al. (2010) and Laurent et al. (1978) studied the parameters affecting the interfacial area in a jet ejector using $CO_2 - NaOH$ system. Both of them have reported similar results that interfacial area increases with increasing liquid velocity up to certain level. There are several investigators who worked on the chemical method for the determination of interfacial area in gas liquid contactors (Raghuram et al., 1992; Oyevaar and Westerterp, 1989; Ogawa et al., 1983; Virkar and Sharma, 1975; Sahay and Sharma, 1973; Volgin et al., 1968).

2.4.3 Determination of overall volumetric mass-transfer coefficient by chemical method

Doraiswamy and Sharma (1984) derived a correlation which may be used to determine the overall volumetric mass-transfer coefficient by chemical method. If the reaction is an irreversible m^{th} order with respect to A and n^{th} order with respect to B , and satisfy the condition

$$\sqrt{M} = \frac{\left(\frac{2}{m+1} D_A k_{mm} [A^*]^{m-1} [B_0]^n \right)^{\frac{1}{2}}}{k_L} \gg 1 \quad (2.28)$$

then the reaction between the gas A and the liquid B can take place entirely in the bulk of the liquid phase and there is negligible reaction occurring in the film. Moreover, if the reaction between the gas component A and the liquid B is sufficiently fast, such that the concentration of un-reacted component A in the bulk of liquid phase is negligible then the absorption rate of gas A per unit volume of the gas-liquid reactor ($R_A a$) can be expressed as

$$R_A a = k_L a [A^*] \quad (2.29)$$

To ensure such condition the reaction should satisfy

$$\frac{k_{mm} [A^*]^{m-1} [B_0]^n}{k_L a} \gg 1 \quad (2.30)$$

Thus if $R_A a$ and the solubility of the gas component A in the liquid phase ($[A^*]$) are known, then the volumetric mass transfer coefficient ($k_L a$) can be experimentally evaluated using the above equation.

2.4.4 Limitations of the chemical method for the determination of mass transfer coefficient

The specific surface area for mass transfer in the gas-liquid contactor is the cumulative area of all the bubbles or drops or film divided by the volume of sample.

However the physical methods of determining interfacial area measure the local Sauter mean diameter and hence local interfacial area. But for practical purposes one need to determine an overall interfacial area for the entire contactor. The chemical method of determining interfacial area makes it possible to determine directly the overall interfacial area over the entire contactor. Charpentier (1982) observed that the difference between the interfacial area measured by the chemical method and photographic method may be due to a small number of large bubbles dominating the interfacial area by the inadvertent exclusion of small bubbles by the photographic method.

Joosten and Danckwerts (1973) introduced correction factor γ which they defined as ratio of increase of liquid absorption capacity to increase of mass transfer due to chemical reaction.

Table 2.8 : Limiting values of θ_0 and E_A for the various chemical regimes used to measure the mass transfer parameters (Midoux et al., 1980)

Regime	$\bar{\phi}_0$	Parameter to determine	Order m	Minimum value of θ_0	Maximum value of E_A
Physical absorption or slow chemical reaction	$\bar{k}_L \frac{\gamma_0}{H_e}$	$k_L a$		3.3	0.25
Intermediary pseudo $(1-n)$ th order chemical reaction	$(\bar{k}_L^2 + D_L k_{1n} (C_B^0)^n)^{\frac{1}{2}} \frac{\gamma_0}{H_e}$	a and $k_L a$	1	4.0	0.20
Rapid pseudo $(1-n)$ th order chemical reaction	$(\frac{2}{m+1} D_L k_{mn} (C_B^0)^n)^{\frac{1}{2}} \left(\frac{\gamma_0}{H_e}\right)^{\frac{(m+1)}{2}}$	a	0	1.35	0.48
			$\frac{1}{2}$	1.80	0.48
			1	2.60	0.30
			2	3.70	0.21
			2	4.80	0.16
Instantaneous chemical reaction	$\bar{k}_L \frac{D_{BL} C_B^0}{D_L z}$	$k_L a$		3.3	0.27
Instantaneous chemical reaction at the interface	$k_G p$	$k_G a$		$\bar{\theta}_D > 20$	0.55

γ_0 = inlet solute gas concentration, ϕ_0 = rate of absorption, $\bar{\theta}_0$ = gas residence time, $\bar{\theta}_D$ = reduced diffusion time, E_A = absorption efficiency.

Due to presence of chemical compound the coalescence rate reduces considerably and hence chemical method may lead to error for the fast coalescing systems. Midoux et al (1980) proposed a flow model for shrinking & non shrinking bubbles. Table 2.8 presents the limiting conditions which can be used to minimize the error in estimating mass transfer parameters by chemical method.

Charpenter (1982) suggested that complimentary conditions proposed by researchers be verified before using their data for scale up.

2.4.5 Effect of the ejector geometry on the mass transfer characteristics

Cramers and Beenackers (2001) investigated the effect of geometrical design parameters like the presence of a swirl device in the upstream section of the nozzle, the mixing tube length and the ratio of nozzle to mixing tube diameter ratio. They observed that all these parameters have significant effect on the mass transfer characteristics. They also studied the influence of gas density on mass transfer characteristics and observed that the volumetric mass transfer coefficient ($k_L a$) increases when higher density gases are used. There are some other researchers who carried out similar studies (Balamurugan et al., 2008, 2007; Gourich, 2007; Baier, 2001). Table (2.9) is comprehensive list and the co-relations given by different investigators (Balamurugan et al., 2007).

Their investigations may be summarized as follows:

Influence of the swirl device

For the same Q_G/Q_L the ejector with swirl device causes higher gas phase pressure difference. The ejector without a swirl device creates higher $k_L a$ values compared to the ejector with a swirl device in the nozzle. The value of $k_L a$ increases with increase in Q_G/Q_L . In case of presence of swirling device, there are two distinguished flow regimes seen viz. bubble flow and annular flow. The ejector without a swirl device creates higher $k_L a$ values as compared to the ejector without swirling device because it utilizes the supplied energy more effectively. In similar study, Zheng et al. (2010) and Baier (2001) (Figure 2.25) concluded that the gas holdup and interfacial area are larger in case of jet ejector without swirl compared to jet ejector with swirl.

Table 2.9 : Hold-up, $k_L a$ and a measurement methods and correlations given by various authors

System	Dimensions (m)	$QG \text{ (m}^3/\text{s)}$	$QL \text{ (m}^3/\text{s)}$	Method of measurement			Correlation	Author
				Hold-up	$k_L a$	a		
Upward, primary—water; secondary—air	$D_N = 0.006 - 0.016$, $D_T = 0.01 - 0.028$, $H_T = 0.05 - 0.26$	5×10^{-5} to 1.3×10^{-3}	0 to 6.6×10^{-4}	2, 3			$\frac{\epsilon_G}{\epsilon_{G0}} = 0.5 \left(\frac{D_N}{D_T} \right)^{-0.3}$ $Fr^{0.3}, \epsilon_{G0} = 0.38 U_G^{*0.84}$, $U_G^* = \frac{U_G}{[\Delta P g \sigma / \rho_L^2]^{1/4}}$	Otake et al. (1981)
Upward, primary—water; secondary—air	Type 1: $D_N = 0.006 - 0.011$, $L = 0.025$ Type 2: $D_N = 0.006$, $L = 0.007$ Type 3: $D_N = 0.008$, $L = 0.0015$, $D_T = 0$, $H_T = 0$, $D_{Dinlet} = 0.0638$, $D_{Doutlet} = 0.159$, $H_D = 0.43$, $D_C = 0.292$	0.28×10^{-3} to 5.04×10^{-3}	0.5×10^{-3} to 2×10^{-3}	1	1		$\epsilon_G = 0.05 e_D^{0.69}$ $\epsilon_D = \frac{\Delta P Q_L}{V_L \rho_L}$ $k_L a = 0.04 e_D^{0.54}$	Zahradnik et al. (1982)
Upward, primary—water; secondary—air	$D_N = 0.006 - 0.010$, $D_C = 0.292$	0.28×10^{-3} to 4.48×10^{-3} , $0.004 - 0.067 \text{ m/s}$	5.5×10^{-4} to $1.8 \times 10^{-3} \text{ m}^3/\text{s}$	1	1		$\epsilon_G = 3.47 U_G$, $k_L a = 2 U_G$	Zahradnik et al. (1982)
Upward, primary—water; secondary—air	$D_N = 0.008$, $D_T = 0.01$, $H_T = 0.225$, $D_C = 0.15$, $H_C = 1.795$	$0 - 1 \times 10^{-3} \text{ m}^3/\text{s}$	$0 - 6.67 \times 10^{-4} \text{ m}^3/\text{s}$	2,4	2	1	$\epsilon_G S_{pout} = 0.346 U_G^{0.55} Fr^{0.3}$, $\epsilon_G C_{aim} = 0.346 U_G^{0.55} Fr^{0.3}$, $0.472 \times 10^{-2} < U_G < 5.6 \times 10^{-2} \text{ m/s}$, $D_B = 1.213 \times 10^{-2}$ $U_G^{0.2} Fr^{-0.375}$, $k_L a S_{pout} = 8.42 \times 10^{-2}$ $U_G^{0.6} Fr^{1.0}$, $k_L a C_{aim} = 0.329 U_G^{0.75} Fr^{0.55}$, $\alpha S_{pout} = 0.285 U_G^{0.36} Fr^{0.8}$, $\alpha C_{aim} = 0.249 U_G^{0.6} Fr^{0.65}$,	Ogawa et al. (1983)
Upward, primary—water; secondary—air	$D_N = 0.008$, $L = 0.025, 0.007, 0.0015$, $D_{Dim} = 0.016$, $D_{Dout} = 0.04$ and 0.028 , $H_D = 0.1 - 0.4$, $D_C = 0.3m$	8.3×10^{-4} to $7.7 \times 10^{-3} \text{ m}^3/\text{s}$, superficial velocity $0.013 - 0.107 \text{ m/s}$	5.5×10^{-4} to $1.8 \times 10^{-3} \text{ m}^3/\text{s}$	1	1		$\epsilon_G = 0.057 e_D^n, n = 0.53$ (for $H_D = 0.4$), $n = 0.42$ (for $H_D = 0.2$), $n = 0.35$ (for $H_D = 0.1$), $k_L a = 0.36 e_D^{0.54}$	Rylek and Zahradnik (1984)
Upward, primary—water; secondary—air							$k_L a = 0.7 \epsilon_G^{1.05}$	Zahradnik et al. (1985)
Downward, primary—water; secondary—air	$D_N = 0.005, 0.008, 0.01, 0.012 \text{ m}$, $D_T = 0.016, 0.0159 \text{ m}$, $D_N/D_T = 1.6 - 3.2$	6.4×10^{-4} to $3.2 \times 10^{-3} \text{ m}^3/\text{s}$	4×10^{-4} to 2.8×10^{-3}	1			$\epsilon_G = A(Q_G)^B$, $A = 0.94 - 2.66$, $B = 0.74 - 1.54$	Bhutada and Pangarkar (1987)

Table 2.9 continued

Continued from previous page

Downward, primary—solution of NaHCO_3 and Na_2CO_3 ; secondary—air + CO_2 mixture	$D_N = 0.0045$, 0.0065 m, $D_T = 0.018$ m, $D_C = 0.040$ m.	0.5×10^{-4} to 3.0×10^{-3}	1×10^{-4} to 5×10^{-4}		3	2	$k_L a = 0.044 \left(\frac{P}{V} \right)^{0.76}$	Dutta and Raghavan (1987)
Upward, primary—sodium sulfite solution, secondary—air	$D_N = 0.003-0.02$, $D_T = 0.01-0.03$, $H_T = 0.05-1.25$	0.25×10^{-3} to 1×10^{-4}	0.3×10^{-3} to 4×10^{-3}		2	1	$\alpha_{\text{pout}} = 15,000 \epsilon^{1.2}$, $\alpha_{\text{catm}} = 7500 \epsilon^{1.1}$	Bando et al. (1990)
Downward, primary—water; secondary—air	$D_N = 0.004-0.006$, $D_T = 0.012$, $D_D = 0.04$	0.9×10^{-4} to 0.24×10^{-2}	0.3×10^{-3} to 0.8×10^{-3}		1		$\frac{k_L a V_{ej}^{\frac{1}{3}}}{D_C} = 5.4 \times 10^{-4}$ $Re^2 \frac{G}{G+L} \cdot 1.3 < \frac{G}{L} < 3$, $\frac{k_L a V_{ej}^{\frac{1}{3}}}{D_C} = 3.1 \times 10^{-4} Re^2$	Dirix (1990)
Downward, primary—water; secondary—air	Not mentioned	$0-7 \times 10^{-3}$	2.8×10^{-4} to 2×10^{-3}	1			$\epsilon_G = 7.7 U_G \left(\frac{\rho_G}{\rho_L} \right)^{0.11}$	Cramers and Dierendonck (1992)
Downward, primary—water; secondary—air	$D_N = 0.009$	2.22×10^{-4} to 3.36×10^{-3}	5.56×10^{-4} to 2.22×10^{-3}			1	$\alpha = 19,500 \left(\frac{P}{V} \right)^{0.4}$ $\epsilon_G (1 - \epsilon_G)^{0.4}$	Cramers and Dierendonck (1992)
Upward, primary—water; secondary—air	$D_N = 0.006-0.012$, $D_T = 0.016$, $D_{\text{out}} = 0.04$	2.78×10^{-4} to 5.1×10^{-3}	5.5×10^{-4} to 2×10^{-3}	2			$\epsilon_G = 2.81 U_G^{0.9}$	Zahradnik et al. (1997)
Upward, primary—water; secondary—air	$D_N = 0.01$, $D_T = 0.018$, $H_T = 0-0.36$	$0-2.33 \times 10^{-3}$	$0-0.083 \text{ m/s}$	2			$\frac{\epsilon_G}{1 - \epsilon_G} = 5.91 U_G^{1.08} \epsilon_B^{0.03}$	Havelka et al. (1997)
Downward, primary—water; secondary—air	$D_N = 0.004, 0.0047$ and 0.0053 , $D_T = 0.012$, $H_T = 0.024-0.120$	$QG/QL = 0-1.5$	Not mentioned			1	$k_L a =$ $C \epsilon_B^{0.65} \epsilon_G^* \left(\frac{\rho_L^2 \rho_G}{\sigma^3} \right)^{0.2} \left(\frac{H_T}{D_T} \right)^{0.42}$ $\left[1 - 0.55 \left(0.38 - \frac{D_N}{D_T} \right)^2 \right]$	Cramers and Beenackers (2001)
Downward, primary—water, CMC; secondary—air	$D_N = 0.004-0.008$, $D_T = 0.019$, $H_T = 0.184$, $H_D = 0.204$, $D_C = 0.0156$	1.11×10^{-6} to 1.89×10^{-5}	9.56×10^{-6} to 2.75×10^{-5}	2			$\epsilon_G = 0.365 Re^{-0.164}$ $\left(\frac{g \mu^4}{\rho \sigma^3} \right)^{-0.029}$ $A_T^{0.032} H_T^{0.207}$	Mandal et al. (2003)
Downward, primary—water; secondary—air	$D_N = 0.004-0.008$, $D_T = 0.019$, $H_T = 0.184$, $H_D = 0.204$	0.83×10^{-4} to 1.58×10^{-3}	0.98×10^{-4} to 2.63×10^{-4}		3	2	$k_L a = 1.08 U_G^{0.92}$, $\alpha = 0.38 \times 10^4 U_G$	Mandal et al. (2003)

Holdup measurement methods: 1. Bed expansion method; 2. difference of static pressure along the column; 3. spark photography for bubble size estimation; 4. photography for bubble size estimation. *Mass transfer estimation measurement methods:* 1. Dynamic method—monitoring of unsteady oxygen absorption into previously deoxygenized water in the bed, i.e. on the evaluation of system response to an input step change nitrogen-air; 2. O_2 absorption in sodium sulfite solution with Cobaltous sulfate as catalyst; 3. absorption of lean CO_2 in the mixture of NaHCO_3 and Na_2CO_3 . *Interfacial area measurement methods:* 1. O_2 absorption in sodium sulfite solution with Cobaltous sulfate as catalyst; 2. absorption of CO_2 in aqueous solution of sodium hydroxide.

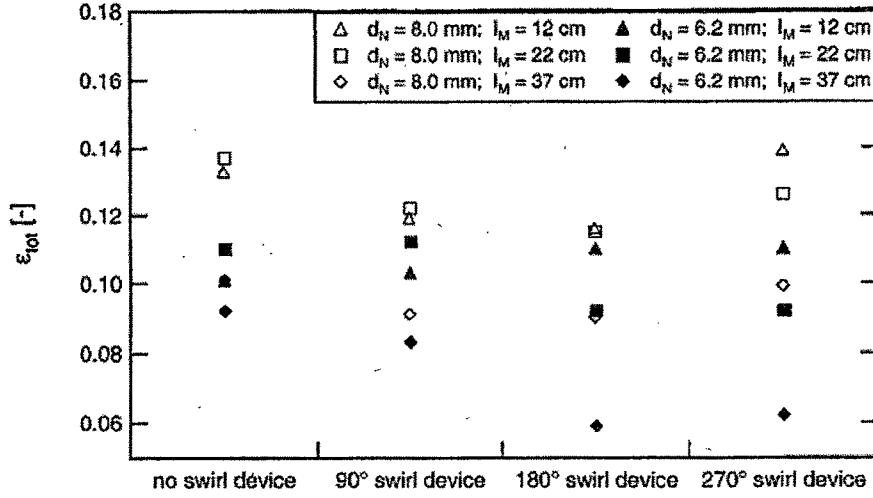


Figure 2.25 : Influence of the swirl device on the total gas holdup (ϵ_{tot})
(Baier, 2001)

Influence of the nozzle to mixing tube diameter ratio (D_N/D_T or A_R)

When using a swirl device $(k_L a)^*$ decreases with increasing diameter ratio. When no swirling device is used then there exists an optimum diameter ratio approximately 0.38. They correlated $(k_L a)^*$ as follow

$$(k_L a)^* \approx \left[\frac{d_N}{d_T} \right]^{0.65} \text{ --- with swirling device} \quad (2.31)$$

and

$$(k_L a)^* \approx 1 - 0.55 \left[0.38 - \frac{d_N}{d_T} \right]^2 \text{ --- without swirling device} \quad (2.32)$$

Influence of the mixing tube length

For the standard ejector ($L_T/D_T = 2$), the mixing zone is located in both the mixing tube and in a large volume of the diffuser. However, when the mixing tube length is increased, it is found that the mixing is nearly completed in the mixing tube. This indicates that the initial dispersion volume (mixing zone volume) is influenced by the ejector configuration. From this visual observation, it can be concluded that the mixing zone volume of an ejector with a L_T/D_T ratio of 10 is smaller compared to the mixing zone volume of an ejector with a shorter mixing tube. They also noted that this observation is in disagreement with the experiment of Dirix and Wiele (1990), the mixing tube length has no influence on $(k_L a)$. (Figure 2.26)

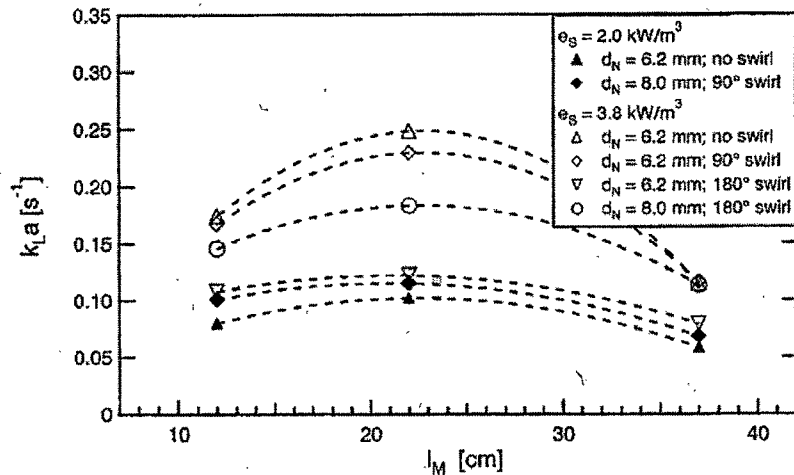


Figure 2.26 : Influence of the mixing tube length on k_La (Baier, 2001)

Utomo et al. (2008) have also studied the effect of mixing tube length on volumetric mass transfer coefficient. They concluded that an ejector with longer mixing tube creates lower volumetric mass transfer coefficient compared to shorter mixing tube. It is seen that by increasing L_T/D_T ratio, the volumetric mass transfer coefficient decreases for any gas liquid flow rate ratios. They also explained that when the mixing tube length is increased, the pressure drop is also increased.

Influence of the gas density on mass transfer characteristics

In the bubble flow regime, the volumetric mass transfer coefficient increases when higher density gases are used. The results could be explained by using Levich's theory, i.e. when the gas density increases, smaller bubbles get dispersed resulting in an increase of the k_La value. (Figure 2.27)

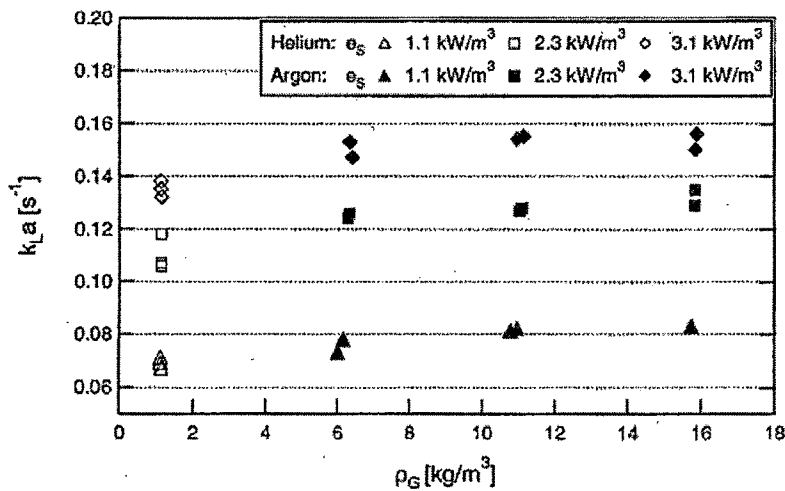


Figure. 2.27: Influence of gas density on k_La without swirl device (Baier, 2001)

Influence of liquid viscosity on mass transfer characteristics

Baier (2001) investigated the effect of viscosity on mass transfer coefficient. They explained that the volumetric mass transfer coefficient decreases with increase in liquid viscosity (Figure 2.28). They compared their results with Terasaka and Hideki (1991), Sedelies et al. (1987) and Stein and Schafer (1984) and found good agreement

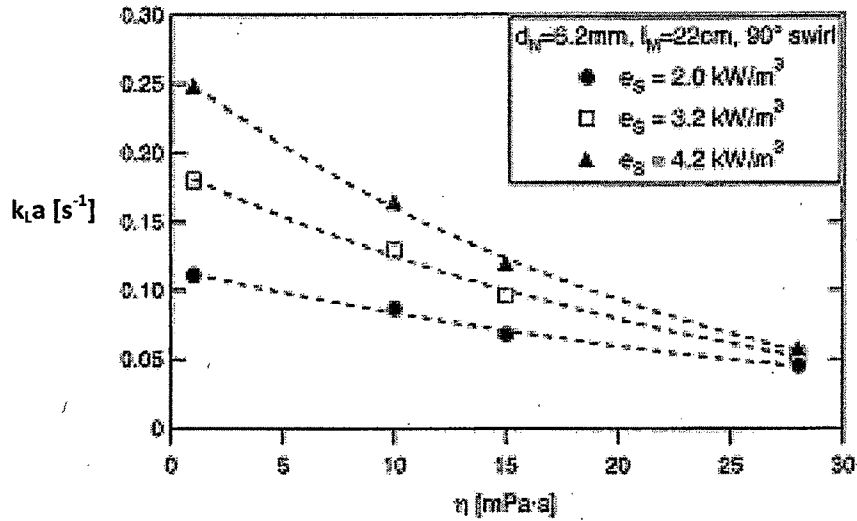


Figure 2.28 : Influence of the liquid viscosity on k_La (Baier, 2001)

2.4.6 Factors effecting mass transfer characteristics

Biswas et al. (1977) studied the effective interfacial area in a liquid jet induced horizontal gas-liquid contactor. They determined the effective interfacial area at various gas liquid throughputs by chemical method. Their results are summarized as follows:

- At same motive liquid flow rate, interfacial area increases with increasing secondary liquid flow rate. Interfacial area is proportional to flow of secondary fluid (gas), Q_S .
- Maximum interfacial area (approx. $2400\text{m}^2/\text{m}^3$) is created by the nozzle having area ratio 9.3
- At same suction gas flow rate, higher interfacial area is achieved by increasing motive fluid flow rate (liquid).
- Interfacial area can be predicted by empirical correlation

$$a = 60 ((\alpha_{GT})/(\alpha_{GO}))^{2.73} (a_R)^{2.33} \quad (2.33)$$

Where α_{GT} is the fraction of gas hold up based on total system volume (dimensionless)

α_{GO} is the fraction of gas holdup at no slip (dimensionless)

- Specific interfacial area produced for same energy/volume to jet ejector is much higher compared to that produced in packed bed, jet contactor and bubble column.

2.4.7 Use of jet ejector in reactor

The use of jet ejector in the loop-reactor has been reported in the literature (Gourich et al., 2007; Tang et al., 2006; Ping-fang Han et al., 2005; Havelka et al., 2000; Dierendonck et al., 1998; Ogawa et al., 1983). These studies have reported about the hydrodynamics and the factors affecting the mass transfer characteristics of the jet ejector used in the different profiles of loop-reactors.

Weisweiler and Rosch (1978) observed that the interfacial area and percentage conversion increase with increasing jet velocity. When jet velocity is increased the conversion increases depending on the gas throughput and at high jet velocity a maximum conversion of nearly 100% is achieved. Liquid jet velocities of less than 10 m/s hardly affect the interfacial area for the dispersion of the gas stream into small bubbles. The liquid jet must be highly turbulent which is ensured when the jet velocity exceeds 10 m/s.

Gourich et al., (2007) and Dierendonck et al., (1998) compared the performance of jet ejector in loop reactor with conventional gas liquid contractors. Their findings were similar to Weisweiler and Rosch (1978) that loop ejector venturi contactors are versatile tools to carry out both fast and slow reactions.

Raghuram (2009) studied interfacial area in gas-liquid ejector for a sodium chloride-air system for a ejector having same nozzle and throat diameter (3mm). They observed that for given flow rate of air and liquid the interfacial area decreases slowly as dispersion is moves away from the nozzle. They also reported that interfacial area increases with increasing liquid to air ratio. They achieved interfacial area of the tune of $5 - 25 \text{ cm}^2/\text{cm}^3$.

Dierendonck et al. (1998) concluded that the loop ejector venturi reactors are an efficient alternative to the stirred tank reactors, offering easier scale-up.

2.4.8 Mass transfer characteristics in multi nozzle jet ejector

Radhakrishnan and Mitra (1984) studied multi nozzle liquid gas ejectors, and observed that optimum ratio of length of throat to diameter of throat is between 6 to 10. Similarly optimum area ratio is from 14.56 to 16.39 and gave the co-relation for gas hold up as

$$(\alpha_1)_{cal} = 1 - \exp(-38.176 X_2) \quad (2.34)$$

$$\text{where } X_2 = A_R^{-0.06} n^{-0.06} Re_{ls}^{0.0002} Re_{gs}^{-0.55} \quad (2.35)$$

Where α_1 is fractional liquid hold up i.e. ratio of liquid volume to the volume of system

n – number of orifices in the nozzle plate Re_{ls} and Re_{gs} are Reynold's numbers based on superficial liquid and gas velocity on the tube diameter.

They reported co-relation for interfacial area of system, a_{sy} :

$$a_{sy} = 225. \alpha_1^{-2.649} \quad (2.36)$$

They also reported that the optimum performance is obtained with nozzle having $A_R = 14.6$, This nozzle gave maximum specific interfacial area per unit energy input.

2.4.9 Mass transfer with chemical reaction

Danckwerts (1970) proposed in agitated film diffusion, convection and reaction proceed simultaneously. To make any useful prediction about the behavior of such systems, it is necessary to use highly-simplified model which simulate the situation sufficiently well for practical purposes without introducing a large number of parameters which are difficult to determine.

There are many hypothetical models to predict the effect of chemical reaction on absorption rate in the literature.

- Whitman's 'Laminar film model' (1923): steady-state diffusion through a stagnant film
- Higbie's 'Systematic surface renewal (penetration) model' (1935): transient absorption into surfaces which are systematically replaced by fresh liquid

- Danckwerts's 'Random surface renewal model' (1951): transient absorption into surfaces which are randomly replaced.

Danckwerts and Kennedy (1954) compared these three models and showed that the three models lead to closely similar predictions about the effect of physico-chemical variables (solubility, diffusivity, reaction rate etc.) on the rate of absorption.

Wall and Beek (1967) compared chemisorption and physical absorption and concluded that chemisorptions is more than physical absorption.

Vieth et al. (1963) derived an equation which describes the mass transfer to a fluid in fully developed turbulent flow in a pipe. They explained that their correlation for mass transfer is identical with the well-known Chilton-Colburn analogy (1934). They extended their analysis to the case of simultaneous mass transfer and irreversible first-order chemical reaction and found that the solution of their correlation is in agreement with the fact reported by Danckwerts and Kennedy (1954) for penetration and film models.

However the studies by Beltran et al. (1998), Danckwerts et al. (1963) and Richards et al. (1964) had compared different models for different systems and have reported the effect of various parameters.

2.4.10 Reaction systems used to characterize mass transfer with chemical reaction

Sadek et al. (1977) proposed a model for the simultaneous absorption of sulfur dioxide and chlorine into mixed acid.

Ravindram and Pyla (1986) also proposed a theoretical model (based on simultaneous diffusion and an irreversible chemical reaction) for predicting the amount of gaseous pollutant removed in a venturi scrubber. For validation of their model they used system of SO_2 and CO_2 absorption in dilute $NaOH$. They found excellent agreement between the results predicted by the model and those experimentally determined.

Chlorine

Chlorine is one of the most polluting gases in process industries. The absorption of chlorine in aqueous solution of sodium hydroxide is commonly commercially practiced method to deal with chlorine pollution. There have been a few studies on the absorption of Cl_2 in to

aqueous sodium hydroxide solution in different gas-liquid contactors. (Roy and Rochelle, 2004; Ashour et al., 1996; Lahiri et al., 1983; Hikita et al., 1973)

Hikita et al. (1973) studied the rate of absorption of pure chlorine into various concentrations of aqueous sodium hydroxide solution at 30°C. They used a liquid-jet column for their research study. They applied penetration theory for gas absorption accompanied by a two-step instantaneous chemical reaction. The experimental results were in good agreement with the theoretical predictions. They termed their model “two reaction-plane model” as shown below:

- Aqueous solution containing $HOCl$ and $NaCl$ ($= Na^+ + Cl^-$) exists in the region between the gas liquid interface and the first reaction plane (region 1 in Figure 2.29),

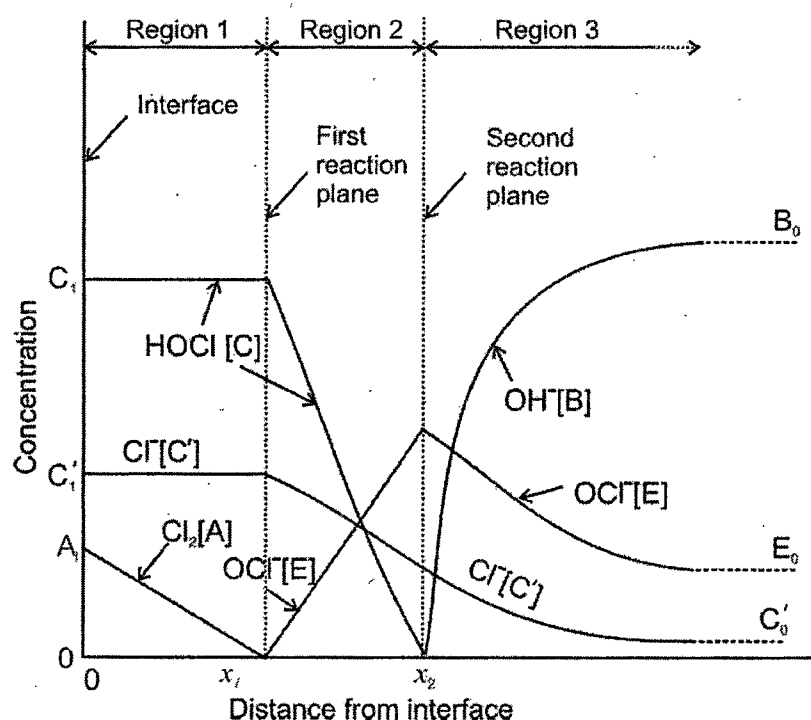


Figure 2.29 : Concentration profiles for absorption of Cl_2 into aqueous $NaOH$ solution (Hikita et al., 1973)

- Aqueous solution containing OCl^- , $HOCl$ and Cl^- exists in the region between the first reaction plane and the bulk of liquid (region 2 in Figure 2.29),

The theoretical predictions and the experimental observations by Spalding and Takahashi et al. are in good agreement.

Tamir et al. (1975) concluded that the neglecting of the effect of the gaseous environment as well as bulk flow contribution is not justified for absorption of gases with high solubilities and large heat effects. They presented a penetration model and validated the model by using the absorption of chlorine into toluene (investigated experimentally by others). They found a deviation of 25% between calculations based on simplified model and the more general model presented by them

Lahiri et al. (1983) deliberated on the absorption of chlorine in aqueous solution of sodium hydroxide with concurrent desorption of hypochlorous acid (followed by its dissociation to chlorine monoxide) at 55°C and 75°C in a stirred contactor with a flat gas-liquid interface. A reasonably good agreement has been found between the theoretical predictions and experimental observations.

Roy and Rochell (2004) measured the absorption rate of chlorine into aqueous solution of sulfite/bisulfite using a stirred-cell reactor and a wetted-wall column in the range pH 4.7 and 5.7. They developed a model using the theory of mass transfer with fast reaction. They also reported that there is enhancement of absorption by using the succinate buffer on the rate of chlorine hydrolysis. They also found that the di-succinate results in greater enhancement of Cl_2 absorption than the mono-succinate anion and the addition of sodium chloride ($NaCl$) as well oxygen did not affect the rate of Cl_2 absorption in S(IV). They opined that these results are relevant in the simultaneous removal of chlorine, sulfur dioxide and elemental mercury from flue gas.

Sulphur dioxide

Uchida and Wen (1973) simulated absorption of SO_2 in H_2O and alkaline solution using a mathematical model developed by them. They compared the calculated results based on their model with experimental data obtained in several types of venturi scrubbers that showed satisfactory agreement.

Charpentier (1976) published a review paper in which he presented. Different theoretical and empirical correlations to calculate $k_L a$ and k_G .

Laurent et al (1978) studied absorption with chemical reaction in venturi jet scrubber. They used slow irreversible reaction to measure $k_L a$ and fast pseudo m^{th} order reaction for $k_G a$.

Asai et al. (1986) analyzed the rate of mass transfer accompanied by chemical reaction of general order proceeding in two continuous phases on the basis of the two-film theory. They could find satisfactory accuracy.

Atay et al. (1987) developed empirical models to describe the fluid flow characteristics and gas absorption efficiency of ejector venturi scrubber. They determined the sulfur dioxide absorption efficiency experimentally on a commercial scrubber.

Bandyopadhyay and Biswas (2007, 2006, 2006a) , studied the removal of SO_2 using water and dilute alkali as scrubbing media in a tapered bubble column scrubber. They observed the enhancement of removal of SO_2 due to presence of particulate matter in the alkali scrubbing media.

Carbon Dioxide

Mandal et al. (2003b) investigated experimentally, a and $k_L a$, in a down flow bubble column by chemical method viz., absorption of CO_2 in aqueous sodium hydroxide and sodium carbonate/bicarbonate buffer solutions respectively. The equipment consists of jet ejector followed by bubble column. They developed correlations to predict a and $k_L a$ in terms of superficial gas velocity by applying Polynomial regression analysis of the experimental data,

$$a = 0.38 \times 10^4 v_{sg} \quad (2.37)$$

and

$$k_L a = 1.80 v_{sg}^{0.92} \quad (2.38)$$

They also compared the experimental data with the predicted values obtained from above equation and found that it fitted very well.

Silva and Danckwerts (1973) studied the effect of adding a small quantity of halogen (chlorine or bromine) to a stream of carbon dioxide on absorption rate of carbon dioxide. The addition of a small quantity of chlorine or bromine increases greatly the rate of absorption of the carbon dioxide into alkaline solutions. This is due to the formation of hypochlorite ion or hypobromite ion in the solution which are catalysts for the reaction between CO_2 and water.

Similar studies were done by using CO_2 -alkali systems by different researchers (Cents, 2005; Gomez and Navaza, 2005; Meikap et al., 2004, 2001; Dimicocoli et al., 2000; Alvarez et al., 1980, 1981; Pohoreckie, 1968; Vidwans and Sharma, 1967; Danckwert and Kennedy, 1958).

Many researchers, (Bhatt et al., 2010, 2007; Gandhi et al., 2009; Ahari et al., 2008; Gulbeyi and Cevdet, 2006; Yusuf et al., 1999; Cooney, 1992, 1985; Yaici et al., 1988; Cooney and Olsen, 1987; Botton et al., 1987; Mahajani and Sharma, 1981, 1980, 1979; Midoux et al., 1984; Ogawa et al., 1983; Charpentier, 1982, 1976; Laurent and Charpentier, 1974; Shende and Sharma, 1974; Volgin et al., 1968; Jhaveri and Sharma, 1968, Danckwerts and Sharma, 1966; Danckwerts and Gillham, 1966; Nijsing et al., 1959) have proposed models to predict absorption with chemical reaction by studying different reaction systems.

Kordac and Linek (2008) studied the effect of addition of salt and super saturation, on the mass transfer coefficient of carbon dioxide-water system. Their experiments show that mass transfer coefficients are enhanced by the effect of liquid super saturation.